Improved Methods For Yang-Mills Spectrum

(Corrected Copy)

Thesis Submitted to
The University of Calcutta
for The Degree of
Doctor of Philosophy (Science)

By
Sourav Mondal

Department of Theoretical Physics
Indian Association for the Cultivation of Science
2A & 2B, Raja S.C.Mullick Road, Jadavpur
Kolkata - 700 032, India

2016

Improved Methods For Yang-Mills Spectrum

Abstract

Understanding the existence of a mass gap in pure Yang-Mills theory is one of the outstanding problems of theoretical physics. This is necessary to explain the short range nature of strong interactions despite the fact that gluons are massless. The spectrum of pure Yang-Mills theory consists of glueballs and the mass of the lightest glueball is supposed to give the mass gap in pure Yang-Mills theory. Using lattice gauge theory calculations one can infer the masses of the glueballs from the long distance behaviour of correlation functions between the states which interact by exchanging glueballs. However, computation of these correlation functions are notoriously difficult in Monte-Carlo simulations. The Signal-to-Noise ratio for correlation functions is very low at large distances and there are contamination due to excited states at small distances. For that reason, it is important to construct efficient methods to compute large distance correlation functions. In this thesis we present an error reduction method based on the multilevel technique for obtaining glueball correlators from Monte Carlo simulations. We consider pure $SU(3)$ gauge theory in $(3+1)$ dimensions with the standard Wilson action. For the update procedure we use three over-relaxation steps for each Cabibbo-Marinari heatbath step. The multi-level along with the multi-hit technique is applied on large loop glueball operators for the scalar and tensor channels. We compare the performance of our method with the ordinary method, and find significant improvement. For the heavier channel we found a greater improvement. For the scalar channel we calculate glueball masses for six different lattice spacings, while for the tensor channels we perform our calculations for five different lattice spacings. Using this method we can follow glueball correlators to temporal separations even up to 1 fermi.

Soumen Mondal.

Abstract

Understanding the existence of a mass gap in pure Yang-Mills theory is one of the outstanding problems of theoretical physics. This is necessary to explain the short range nature of strong interactions despite the fact that gluons are massless. The spectrum of pure Yang-Mills theory consists of glueballs and the mass of the lightest glueball is supposed to give the mass gap in pure Yang-Mills theory. Using lattice gauge theory calculations one can infer the masses of the glueballs from the long distance behaviour of correlation functions between the states which interact by exchanging glueballs. However, computation of these correlation functions are notoriously difficult in Monte-Carlo simulations. The Signal-to-Noise ratio for correlation functions is very low at large distances and there are contamination due to excited states at small distances. For that reason, it is important to construct efficient methods to compute large distance correlation functions. In this thesis we present an error reduction method based on the multilevel technique for obtaining glueball correlators from Monte Carlo simulations. We consider pure $SU(3)$ gauge theory in $(3+1)$ dimensions with the standard Wilson action. For the update procedure we use three over-relaxation steps for each Cabibbo-Marinari heatbath step. The multi-level along with the multi-hit technique is applied on large loop glueball operators for the scalar and tensor channels. We compare the performance of our method with the ordinary method, and find significant improvement. For the heavier channel we found a greater improvement. For the scalar channel we calculate glueball masses for six different lattice spacings, while for the tensor channels we perform our calculations for five different lattice spacings. Using this method we can follow glueball correlators to temporal separations even up to 1 fermi.

To My Parents

Acknowledgment

Working for a Ph.D. degree is one of the most transforming chapters of an academician's life. During my voyage as a student of Physics, I was fortunate enough to come across many individuals without whose help and inspiration it would have been impossible for me to reach this stage. I would like to take this opportunity to thank them for their help, guidance and advice. I have no words to express my gratitude to the members of the Department of Theoretical Physics of my home institute. First and foremost, I am thankful to my supervisor Dr. Pushan Majumdar, who was most helpful at every stage of my Ph.D. His guidance and training made it possible to come this far. His patience for my queries and problems, analysis of my performance, spontaneous and constant motivation inspired me to produce my best. I am also grateful to Prof. Sourov Roy, Prof. Utpal Chattopadhyay, Prof. Koushik Ray, Prof. Dilip Kumar Ghosh, Prof. Soumitra SenGupta, Prof. Sudhansu Sekher Mandal and Prof. Krishnendu Sengupta of the same group for their encouragement, spontaneous affection, crucial guidance and of course criticism, in academics and life beyond it.

I am thankful to Prof. Nilmani Mathur (TIFR, Mumbai) for giving me opportunity to work with him. His valuable comments and suggestions enabled me to improve my works.

It is my duty to express my sincere gratitude to all of my teachers, starting from the very basic level till date. It was their kind and hard efforts which help me to reach here. I would like to express my gratitude to Dr. Krishnendu Mukherjee for his precious guidance and unconventional teaching during my post-graduate studies. I am really fortunate enough to receive his affection and guidance till date.

I also express my humble thanks to my home institute, Indian Association for the Cultivation of Science, for providing all the facilities like high-performance personal desktop, constant and affluent access to high-speed internet, a homely atmosphere and definitely a world class library. I am also thankful to all the non-teaching staff members of my department (Mr. Subrata Balti, Mr. Bikash Darji, Mr. Bhudeb Ghosh, Mr. Tapan Moulik and Mr. Suresh Mondal) who were always there to assist us.

It is a pleasure to express my thanks to my colleagues and friends who were always there to cheer me up when things were not so smooth either in academics or in personal life. My cordial and special thanks to Dr. Naba Kumar Bera, Dr. Pradipta Ghosh, Dr. Jaydip Mitra, Dr. Debottam Das, Dr. Sudipto Paul Chowdhury, Dr. Dwipesh Majumder, Dr. Kush Saha, Dr. Subhadeep Mondal, Dr. Sanhita Modak, Dr. Shreyoshi Mondal, Dr. Ashmita Das, I am really thankful to them and also to Dr. Amit Chakraborty, Sabyasachi Chakraborty, Sutirtha Mukherjee, Manimala Chakraborty, Anirban Datta, Ipsita Saha, Abhishek Dey, Saurav Nandy, Bhaskar Mukherjee, Asmi Haldar, Hiya Mukherjee, Heerak Banerjee, Nibedita Ghosh making my office my second home.

Finally, I would like to thank my family for all their love and inspiration, specially my parents for supporting me and always remaining by my side; without their help it would never have been possible for me to reach this stage in my life.

Sourav Mondal

List of Publications

In refereed journals.

- Noise reduction algorithm for Glueball correlators
  Phys. Lett. B 736 (2014) 415
  arXiv:hep-lat 1403.2936
  [Pushan Majumdar, Nilmani Mathur, Sourav Mondal].

In proceedings.

- Light Glueball masses using the Multilevel Algorithm.
  PoS (LATTICE2014) 039
  arXiv:hep-lat 1411.3503
  [Sourav Mondal, Pushan Majumdar, Nilmani Mathur]

Contents

Chapter 1

Introduction

Quantum Chromodynamics (QCD) is expected to be the fundamental theory of strong interactions. QCD provides a model of quarks interacting through the exchange of gauge bosons charged under a $SU(3)$ gauge group. In this theory each quark carries one of the three possible fundamental $SU(3)$ charges (say red, green or blue) commonly known as color charges. The gauge bosons belonging to the adjoint representation of $SU(3)$ are known as gluons (G^a_μ). The quarks can change color by emitting gluons. The quark model provides for substructure within hadrons and describes the properties of hadrons in terms of quarks and gluons.

In QCD the coupling strength for exchange of a gluon between two quarks is given by

$$\Big(\frac{C_1}{\sqrt{2}}\Big)\Big(\frac{C_2}{\sqrt{2}}\Big)\alpha_s \tag{1.1}$$

where C_1 and C_2 are color coefficients associated with the two vertices for the gluon exchange [2] and $\alpha_s = \frac{g_s^2}{4\pi}$ with g_s being the strong coupling coefficient.
The lagrangian density of QCD which describes the properties, symmetries and interactions between the fundamental constituents of the theory can be written as,

$$\mathcal{L} = \overline{\psi}\big(i\gamma^\mu D_\mu - m\big)\psi - \frac{1}{2}Tr\big[F^{\mu\nu}F_{\mu\nu}\big] \tag{1.2}$$

where $D_\mu = \partial_\mu + igA_\mu$ and $F_{\mu\nu}(x) = \partial_\mu A_\nu(x) - \partial_\nu A_\mu(x) + ig\big[A_\mu(x), A_\nu(x)\big]$ with $A_\mu(x) = A^a_\mu t^a$, t^a being the generators of the SU(3) algebra.

In QCD the effective coupling constant behaves differently than quantum electrodynamics. The reason behind that is the gluons carry color charges and they interact with each other. In the one-loop approximation, the QCD coupling varies with the

renormalization scale μ as,

$$\alpha_s(\mu) = \frac{4\pi}{\beta_0 \ln\left(\frac{\mu^2}{\Lambda^2_{QCD}}\right)} \tag{1.3}$$

where Λ_{QCD} is a QCD scale and β_0 is the one loop beta function. So, the coupling becomes small at large μ or short distances. This phenomena is known as asymptotic freedom.

The unique feature of the underlying quantum field theory which makes the perturbative approach useful in QCD is asymptotic freedom. Experimental verifications of these features signify the success of the perturbative QCD.

The deep inelastic scattering (DIS) of leptons on hadrons played a crucial role in the development of the parton model and QCD. DIS of charged and neutral lepton on hadrons with exchange of a vector boson can be expressed as

$$l_1(k) + A(p) \rightarrow l_2(k') + X \tag{1.4}$$

where A is a hadron, $l_{1,2}$ are leptons, and X represents the summed-over final state hadronic particles. The scale dependence of the partonic distribution function (PDF) can be calculated using perturbative QCD. This dependence has been verified experimentally with a very high degree of accuracy. The neutral current structure function $F_2(x, Q)$ measured in fixed target experiments SLAC, BCDMS, NMC and collider experiments H1, ZEUS [17] is given Fig. 1.1 along with corresponding NLO QCD results.

Despite of the success of QCD as a field theory with color degrees of freedom an isolated quark never appears as a free particle emerging from an experiment, which suggests that a colored particle cannot appear as an isolated particle in final states. This phenomena is known as color confinement.

For momenta of the order of 1 GeV the QCD coupling becomes too large for perturbation theory to work see Fig. 1.2. Due to the strong coupling, a quantitative description of the confinement problem and computation of the hadron spectrum are difficult in QCD. The description of long distance strong color forces require non-perturbative techniques. Lattice gauge theory formulation is a systematic non-perturbative technique for QCD calculations. Prediction of the non-perturbative evolution of QCD coupling has been a major success of lattice gauge theory and currently the most accurate determination of α_s at the Z_{mass} is from calculation in lattice gauge theory [1]. Lattice gauge theory was formulated by K. G. Wilson [1]. In this formulation the theory is defined on a Euclidean space-time lattice. The lattice provides a cutoff removing

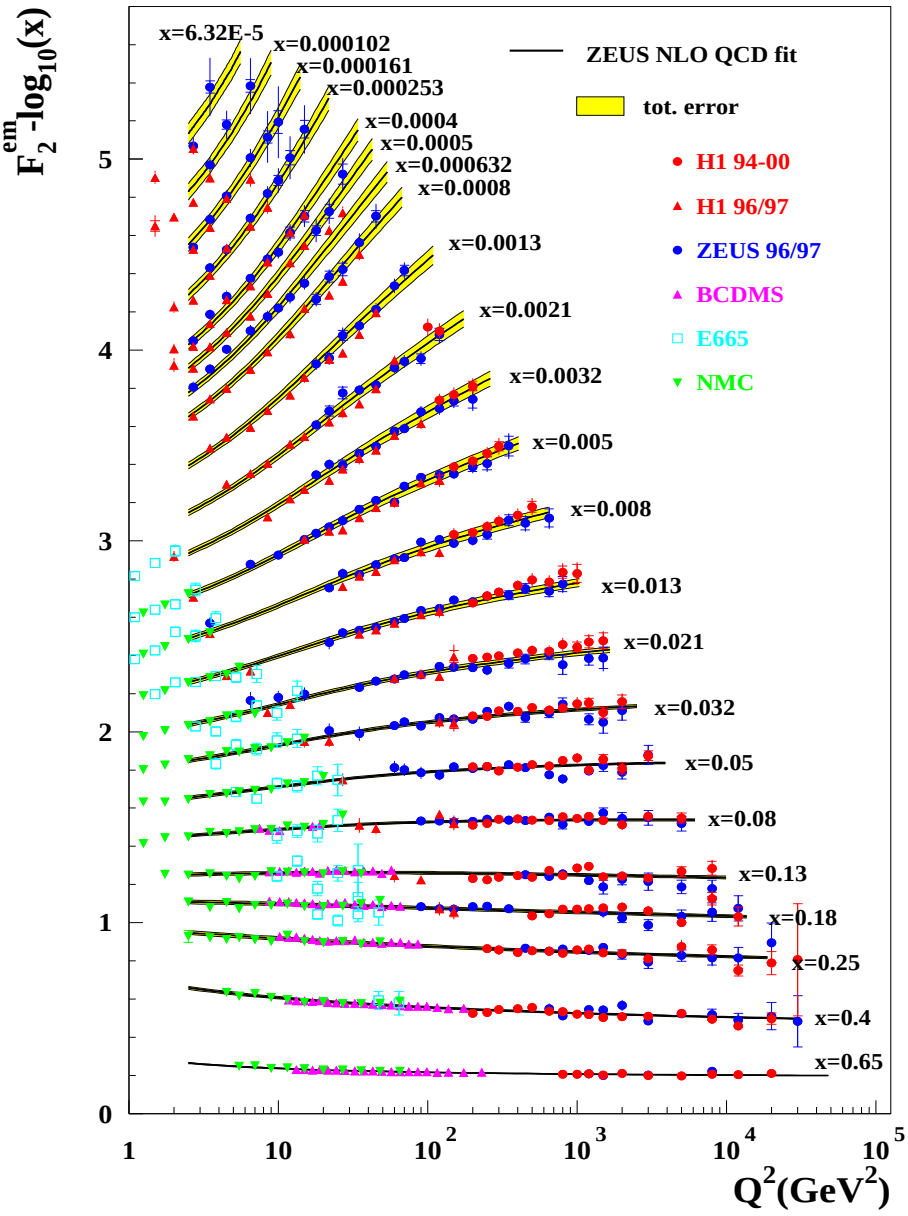

Figure 1.1: $F_2(x, Q)$ from pure γ exchange, from HERA and fixed target experiments compared with NLO QCD. Figure taken from [17].

ultraviolet divergences of the underlying Quantum Field Theory by directly eliminating all wavelengths less than twice the lattice spacing. As with any other regulator, the lattice cutoff must be removed after renormalization. While the confinement property of QCD can be demonstrated in the strong coupling limit of lattice gauge theory, the region of physical interest i.e. the continuum limit lies in the weak coupling region.

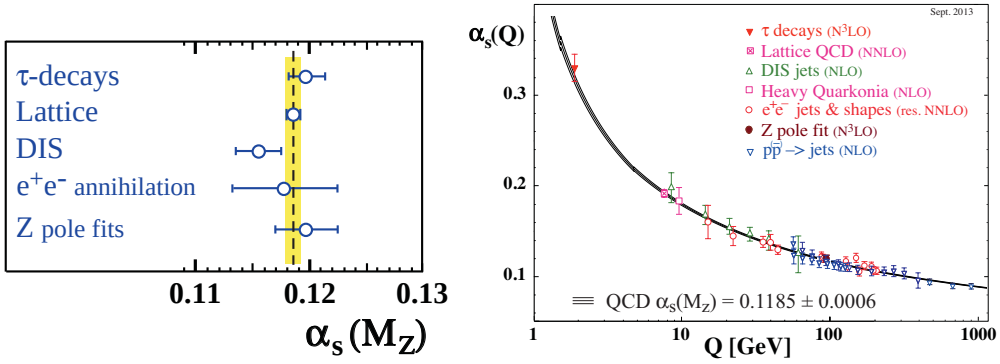

Figure 1.2: QCD running coupling [1].

Gauge invariance forbids a mass term for the gauge boson and in QCD as well as in pure Yang-Mills theory (gauge part of QCD) the gluon propagator remains mass less to all orders in perturbation theory. Nevertheless the strong force is short ranged. This means that the lowest eigenstate of the Hamiltonian above the vacuum has a mass m. Gluon self-coupling in Yang-Mills theory suggests the existence of bound states of gluons. Stable low-lying states in pure Yang-Mills theory are called glueballs, which are characterised by their spin J, parity P and charge conjugation C. In QCD quarks allow glueballs to decay but their signature is expected to remain in the QCD spectrum.

Glueball masses can be computed in lattice quantum chromodynamics and a lot of effort has been directed towards this computation. However there is still no consensus regarding the mass spectrum. It is a difficult computation in lattice QCD with dynamical fermions due to the high masses of the glueballs (>1 GeV) and their mixing with mesonic operators involving quark fields in the same symmetry channels. In recent times computations of glueball masses in lattice QCD with dynamical fermions have been attempted in Refs. [4–6]

Glueball masses are often computed in pure Yang-Mills theory. Advantages are that there is no mixing with mesonic operators and the glueballs are stable as they cannot decay. Thus it is much easier to extract the glueball masses from Monte Carlo simulations of pure Yang-Mills theory than lattice QCD with dynamical fermions. Nevertheless, even in this theory, glueball correlation functions are dominated by statistical noise at large temporal separations and contribution from excited states at short separations. Global fits become difficult and one often computes the "effective mass" which is the logarithm of the ratio of the values of the correlation function between successive time slices. If the effective mass does not vary over a significant temporal range then

one assumes that the effective mass is the same as the globally fitted mass.

To remove the effect of excited states, conventional methods involve computing correlation matrices with matrix elements between a large set of interpolating operators constructed from smeared or fuzzed links [7] in the relevant symmetry channel. The ground state is obtained by diagonalizing the correlation matrix in each channel [8]. As it is difficult to follow the correlator signal to large physical distances, even using the above techniques, one often uses asymmetric lattices with a significantly smaller temporal spacing compared to the spatial lattice spacing with the expectation to observe a flat behaviour of the effective masses [9, 10] over several time slices.

A different approach is to use noise reduction algorithms. Such algorithms have been used in the past for computing the glueball spectrum for $U(1)$, $SU(2)$ and $SU(3)$ lattice gauge theories [11–16].

In this thesis we follow the latter approach. We restrict ourselves to pure Yang-Mills theory with gauge group $SU(3)$ and employ only the standard operators in each J^{PC} channel (scalar and tensor) but try to follow the correlator to large temporal separations using a new noise reduction algorithm. Since the contamination due to excited states falls off exponentially, we expect correlators at distances beyond 0.5 fermi to be dominated by the ground state.

Bibliography

[1] J. Beringer *et al.* [Particle Data Group] *Phys. Rev. D* **86** (2012) 010001.

[2] F. Halzen and A. D. Martin, *Quarks and Leptons*, *John Wiley & Sons.* (1984).

[3] K. G. Wilson, *Phys. Rev.* **D10** (1974) 2445.

[4] A. Hart, M. Teper, UKQCD Collaboration, *Phys. Rev.* **D65** (2002) 034502.

[5] A. Hart, et al., UKQCD Collaboration, *Phys. Rev.* **D74** (2006) 114504.

[6] C. M. Richards, et al., UKQCD Collaboration, *Phys. Rev.* **D82** (2010) 034501

[7] M. Teper, *Phys. Lett.* **B183** (1987) 345.

[8] G. S. Bali, et al., UKQCD Collaboration, *Phys. Lett.* **B309** (1993) 378.

[9] C.J. Morningstar, M.J. Peardon, *Phys. Rev.* **D60** (1999) 034509.

[10] Y. Chen, et al., *Phys. Rev.* **D73** (2006) 014516.

[11] H.B. Meyer, *JHEP.* **0301** (2003) 048.

[12] H. B. Meyer, *JHEP.* **0401** (2004) 030.

[13] P. Majumdar, Y. Koma, M. Koma, *Nucl. Phys.* **B677** (2004) 273.

[14] H.B. Meyer, *JHEP.* **0901** (2009) 071.

[15] H.B. Meyer, M.J. Teper, *Phys. Lett.* **B605** (2005) 344.

[16] M. Della Morte, L. Giusti, *JHEP.* **1105** (2011) 056.

[17] N. Werner [H1 and ZEUS ollaborations], `[arXiv:hep-ex/0305109]`.

Chapter 2

Lattice Gauge Theory

Lattice gauge theory is gauge theory formulated on an Euclidean space-time lattice. The Euclidean path integral on the lattice is used as a tool to quantize the fields. The lattice formulation emphasizes a close connection of Quantum Field Theory with statistical mechanics. The path-integral on an Euclidean space-time lattice is equivalent to a partition function of an analogous statistical system. This chapter is concerned with this connection and a short introduction to lattice discretization technique of continuum Yang-Mills theory.

2.1 Feynman Path Integral on Lattice

In Feynman's functional approach [1] of Quantum Mechanics the path integral is defined as a limit of a finite dimensional integral resulting from a discretization of time.

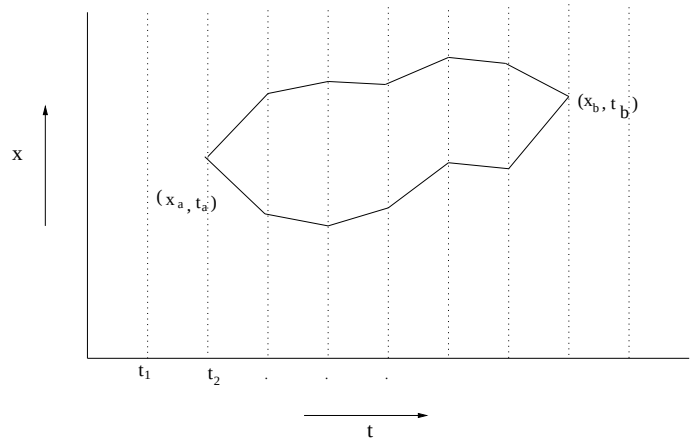

In this approach the probability that a system will be at x_b at time t_b which was

initially at x_a at time t_a, is given by

$$\langle x_b, t_b | x_a, t_a \rangle = \langle x_b | \exp[-iH(t_b - t_a)] | x_a \rangle = \int_{x(t_a)}^{x(t_b)} \mathcal{D}x(t) \exp(-iS[x(t)]) \tag{2.1}$$

where $\mathcal{D}x$ is a measure on the set of paths with starting point x_a at t_a and end point x_b at t_b and the integral is over all such paths. For each path considered, S is classical action computed along that path. Thus each possible path contributes to the transition amplitude weighted by a factor $\exp(iS[x])$. (Here we set $\hbar = 1$, otherwise the weight factor is $\exp(iS[x]/\hbar)$.)

Analogously, in the functional integral approach of Quantum Field Theory, the functional integral for a free scalar field theory is defined as,

$$Z = \int \mathcal{D}\phi \exp(iS[\phi]) \tag{2.2}$$

$S[\phi]$ being the scalar field action

$$S[\phi] = \frac{1}{2} \int dt d^3x [\partial^\mu \phi \partial_\mu \phi - m^2 \phi^2] \tag{2.3}$$

The integral measure $\mathcal{D}\phi$ implies that the integral is taken over the fields at every point in space-time lattice.

After a Wick rotation to imaginary time,

$$t \to -i\tau \tag{2.4}$$

$$iS[\phi] \to -S_E[\phi] \tag{2.5}$$

The Euclidean functional integral now becomes

$$Z_E = \int \mathcal{D}\phi \exp(-S_E[\phi]) \tag{2.6}$$

where

$$S_E[\phi] = \frac{1}{2} \int d^4x [(\partial_\mu \phi)^2 + m^2 \phi^2]. \tag{2.7}$$

To formulate the lattice version of the Euclidean functional we introduce four dimensional hypercubic lattice Λ such that,

$$\Lambda = a\mathbf{Z}^4 = n | \frac{n_\mu}{a} \in \mathbf{Z} \tag{2.8}$$

where a is the lattice constant. The scalar fields $\phi(n)$ are defined on the lattice points n, where $n \in \Lambda$. On the lattice

$$\int d^4x \to a^4 \sum_n \tag{2.9}$$

which implies that the fields are now summed over discrete lattice points and the derivative $\partial_\mu \phi(x)$ is replaced by the finite difference. In symmetric derivative definition

$$\partial_\mu \phi(n) = \frac{1}{2a}[\phi(n + a\hat{\mu}) - \phi(n - a\hat{\mu})]. \tag{2.10}$$

There exist other definitions for these derivatives which will produce same continuum limit. In this thesis we will consider the symmetric definition of the derivative.

The Euclidean path integral plays the role of partition function of an equivalent statistical system, where the Euclidean action plays the role of Hamiltonian of the statistical system.

In lattice discretization of QCD, fermionic fields are placed on the lattice sites n. Under the local gauge transformations the fermionic fields transform as

$$\psi'(n) = V(n)\psi(n) \tag{2.11}$$

$$\overline{\psi}'(n) = \overline{\psi}(n)V^\dagger(n) \tag{2.12}$$

where $V(n)$ is an element of $SU(3)$ for each lattice site n. The discretized version of continuum Dirac action is

$$S_F[\psi, \overline{\psi}] = a^4 \sum_{m,n\in\Lambda} \sum_\mu \overline{\psi}(n)(D_\mu^{lat}(m,n) + m\delta_{m,n})\psi(m) \tag{2.13}$$

where $D_\mu^{lat}(m,n)$ can be one of the various lattice Dirac operators such as the the Wilson Dirac operator, the staggered Dirac operator, the domain wall operator or the overlap Dirac operator to name a few.

Gauge invariance of the fermion action requires a gauge field $U_\mu(n)$ which transforms under local gauge transformation as

$$U_\mu{}'(n) = V(n)U_\mu(n)V^\dagger(n + \mu). \tag{2.14}$$

The gauge field $U_\mu(n)$ is defined on the bond between the sites n and $n + \mu$ and are commonly called link variables. The link variable can be associated with the continuum gauge field by identifying $U_\mu(n)$ with the parallel transporter $U(\mathcal{C}_{xy})$.

$$U(\mathcal{C}_{xy}) = P \exp[-i \int_{\mathcal{C}_{xy}} dz_\mu \mathcal{A}_\mu(z)] \tag{2.15}$$

where P denotes the path ordering and the $\mathcal{A}_\mu(z)$ denotes the continuum gauge fields. On the lattice, the gauge fields $A_\mu(n)$ are held constant along the link and the variable can be written as

$$U_\mu(n) = \exp(iaA_\mu(n)), \tag{2.16}$$

where $A_\mu(n)$ belongs to the SU(3) algebra, as long as $U_\mu(n)$ is continuously connected to identity.

2.2 Lattice Gluon Action

In the last section we introduced the gluonic field variables $U_\mu(n)$. In order to construct the pure-gauge part of the QCD action on the lattice we need gauge invariant objects made entirely out of link variables.

Using the gauge transformation properties of the link variables we can construct gauge invariant objects by using path ordered product of link variables along closed loops. Let $W[U]$ be the path ordered product of link variables on a closed path $\mathcal{C}$ on the lattice.

$$W[U] = tr[\prod_{(n,\mu)\in\mathcal{C}} U_\mu(n)]. \tag{2.17}$$

From eq. 2.14 it is clear that the gauge rotations at the end points of the link variables are cancelled by the gauge rotations of neighbouring link variables around a loop.

These loops are known as Wilson loops. The simplest such Wilson loop, consisting of four links is known as the plaquette

$$U_{\mu\nu}(n) = U_\mu(n)U_\nu(n+\mu)U_\mu^\dagger(n+\nu)U_\nu^\dagger(n). \tag{2.18}$$

For small a we can expand the link variable (2.16) as,

$$U_\mu(n) = 1 + iaA_\mu(n) + O(a^2). \tag{2.19}$$

Using expansion (2.19) and the Baker-Campbell-Hausdorf formula one can get the expansion for the plaquette,

$$U_{\mu\nu}(n) = \exp\left(ia^2(\partial_\mu A_\nu(n) - \partial_\nu A_\mu(n) + i[A_\mu(n), A_\nu(n)]) + O(a^3)\right). \tag{2.20}$$

In Wilson's formulation, gauge action on the lattice is defined as

$$S_G[U] = \frac{2}{g^2} \sum_{n\in\Lambda} \sum_{\mu<\nu} Re\ tr[1 - U_{\mu\nu}(n)]. \tag{2.21}$$

It immediately follows from (2.21) that for small a

$$\frac{2}{g^2} \sum_{n\in\Lambda} \sum_{\mu<\nu} Re\ tr[1 - U_{\mu\nu}(n)] = \frac{a^4}{2g^2} \sum_{n\in\Lambda} \sum_{\mu,\nu} (tr[F^2_{\mu\nu}(n)] + \mathcal{O}(a^2)), \tag{2.22}$$

where the $O(a^2)$ term in the expansion of exponential (2.20) cancels out when taking the real part.

After having defined lattice field variables and the Wilson gauge action the next step to quantize gauge fields is to specify the functional integral. On lattice the expectation value of some observable O is given by

$$\langle O \rangle = \frac{1}{Z} \int D[U] \exp(-S_G[U]) O[U] \tag{2.23}$$

where the partition function Z is defined as

$$Z = \int D[U] \exp(-S_G[U]). \tag{2.24}$$

The integration measure for the link variable is a product measure

$$\int D[U] = \prod_{n\in\Lambda} \prod_{\mu=1}^{4} \int dU_\mu(n). \tag{2.25}$$

$\int dU_\mu(n)$ for each link is a volume in group space. The total volume of the group space is finite for a compact group and therefore the partition function Z, for a finite lattice is well defined.

If the fermionic fields are present, the corresponding measure has to be included in the integral

$$\langle O \rangle = \frac{1}{Z} \int D[\psi, \overline{\psi}] D[U] \exp(-S_F[\psi, \overline{\psi}, U] - S_G[U]) O[\overline{\psi}, \psi, U]. \tag{2.26}$$

Restricting ourselves to the pure-gauge sector of the theory we will consider only the (2.23) for the definition of observables on the lattice.

The Wilson gauge action $S_G[U]$ is invariant under the gauge rotations of the link variables

$$S_G[U'] = S_G[U]. \tag{2.27}$$

The partition function Z should remain gauge invariant as the theory remains invariant under gauge transformations and as for any integral, the resulting functional integral should also remain invariant under the change of variables. This implies

$$Z = \int D[U] \exp(-S_G[U]) = \int D[U'] \exp(-S_G[U']) = \int D[U'] \exp(-S_G[U]) \quad (2.28)$$

therefore the gauge field measure must be gauge invariant

$$D[U] = D[U']. \quad (2.29)$$

As $D[U]$ is a product measure we get, for the integration over the individual gauge link

$$dU_\mu(n) = dU'_\mu(n) = d(V(n)U_\mu(n)V^\dagger(n+\mu)) \quad (2.30)$$

where the group valued matrices $V(n)$ can be chosen independently at each lattice site. The gauge transformations of the link variables can be written as left and right translation in group space,

$$U' = VU, \quad \text{left}, \quad (2.31)$$

$$U' = UV, \quad \text{right}. \quad (2.32)$$

The Haar measure is invariant under such translations in group space. Using the coordinates α in group space $U = \exp(i\alpha^a t^a)$ the Haar measure can be written as [3],

$$dU = \nu \sqrt{det\ g} \prod_k d\alpha^k, \quad (2.33)$$

where the metric g in coordinate space, is of the form

$$g_{kl} = \frac{1}{\rho}\ tr\left(\frac{\partial U}{\partial \alpha^k}\frac{\partial U^\dagger}{\partial \alpha^l}\right), \quad \rho = \frac{1}{2}, \quad (2.34)$$

The normalization factor ν is chosen in such a way that

$$\int dU = 1. \quad (2.35)$$

The metric (2.34) is covariant under the transformation $\alpha^k = f^k(\alpha')$,

$$g_{kl} = g_{mn}\frac{\partial \alpha'^m}{\partial \alpha^k}\frac{\partial \alpha'^n}{\partial \alpha^l} \quad (2.36)$$

The Jacobian factors cancels out and one gets $dU' = dU$. Since the left and right translations are special cases of coordinate transformations, the measure is invariant under these translations,

$$dU = d(VU) = d(UV). \quad (2.37)$$

Bibliography

[1] R. P. Feynman, *Rev. Mod. Phys.* **20** (1948) 367.

[2] K. G. Wilson, *Phys. Rev.* **D10** (1974) 2445.

[3] R. Gilmore, *"Lie Groups, Lie Algebras and Some of Their Applications"*, (John Wiley & Sons, New York).

Chapter 3

Glueball Spectrum

Physical states in the Hilbert space of lattice gauge theory are gauge invariant. They can be obtained by applying gauge invariant operators on the lattice gauge theory vacuum. Let θ_i be a set of gauge invariant operators, the generic wave function is obtained as a linear combination

$$|\psi\rangle = \sum_i c_i \theta_i |0\rangle \tag{3.1}$$

where $c_i \in \mathbb{C}$. The gauge invariant operators are functions of the basic variables of the theory. Restricting ourselves to pure gauge theory without fermionic fields, the operators are gauge invariant functions of the link variables only. Particular candidates can be constructed using traces of parallel transporter around closed loops

$$O_i(x,t) = tr(\prod_{\mathcal{C}_i} U) \tag{3.2}$$

Here tr implies trace over some representation and $\mathcal{C}_i$ implies ith closed loop. The product of link variables around closed paths are known as Wilson loops. As discussed earlier, the simplest among them are known as plaquettes. One can construct zero momentum operators on different time slices by taking sum over all spatial Wilson loops in a time slice. We will show in this chapter that glueball masses can be extracted from the correlators of these operators.

3.1 Transfer Matrix

Using the fact that the transfer matrix [1–3] of a lattice model provides the relation between the functional integral and the Hamiltonian we will use the the transfer matrix formulation of lattice gauge theory to extract glueball masses from the connected

correlators of the operators.

Let us first denote the set of links that are completely contained in time slice $x_4 = t$ by $\mathcal{U}_t$ and those links which connect the time slices $x_4 = t$ and $x_4 = t + 1$ by $\mathcal{U}_{t+1,t}$. Using this notation the action can be written as

$$S = \sum_t L[\mathcal{U}_{t+1}, \mathcal{U}_{t+1,t}, \mathcal{U}_t] \tag{3.3}$$

The transfer matrix can be defined with matrix elements

$$T[\mathcal{U}_{t+1}, \mathcal{U}_t] = \int D[U]_{U \in \mathcal{U}_{t+1,t}} \exp\{-L[\mathcal{U}_{t+1}, \mathcal{U}_{t+1,t}, \mathcal{U}_t]\} \tag{3.4}$$

The transfer matrix acts on the square integrable wave functions ψ_t at a fixed time t and takes it to the time $t + 1$

$$|\psi_{t+1}\rangle = \mathbb{T}|\psi_t\rangle. \tag{3.5}$$

In terms of the transfer matrix the partition function for a lattice which extends over N_t units in the time direction with periodic boundary condition, is given by

$$Z = tr\left(\mathbb{T}^{N_t}\right). \tag{3.6}$$

The correlation functions of the operators in terms of $\mathbb{T}$ can be written as

$$\langle O_2(t)O_1(0)\rangle = \lim_{T\to\infty} \frac{tr\left(\mathbb{T}^{N_t - n_t}\hat{O}_2\mathbb{T}^{n_t}\hat{O}_1\right)}{tr(\mathbb{T}^{N_t})}, \tag{3.7}$$

where $T = aN_t$ and $t = an_t$. The Hamiltonian H on lattice is defined by

$$\mathbb{T} = \exp(-aH) \tag{3.8}$$

Inserting complete set of eigenstates of the lattice Hamiltonian in (3.7) yields [8]

$$\langle O_2(t)O_1(0)\rangle = \frac{\sum_{m,n}\langle m|e^{-(T-t)H}\hat{O}_2|n\rangle\langle n|e^{-tH}\hat{O}_1|m\rangle}{\sum_n\langle n|e^{-TH}|n\rangle} \tag{3.9}$$

$$= \frac{\sum_{m,n} e^{-(T-t)E_m}\langle m|\hat{O}_2|n\rangle e^{-tE_n}\langle n|\hat{O}_1|m\rangle}{\sum_n e^{-TE_n}} \tag{3.10}$$

$$= \frac{\sum_{m,n}\langle m|\hat{O}_2|n\rangle\langle n|\hat{O}_1|m\rangle e^{-t\Delta E_n}e^{-(T-t)\Delta E_m}}{1 + e^{-T\Delta E_1} + e^{-T\Delta E_2} + ...}, \tag{3.11}$$

where $\Delta E_n = E_n - E_0$. The Euclidean correlator $\langle O_2(t)O_1(0)\rangle$ depends only on the energies normalized relative to the energy E_0 of the vacuum. From now on we denote

M_n as the energy differences relative to the vacuum. In the $T \to \infty$ limit the denominator in (3.11) becomes 1 and in the numerator the only contribution comes from the term $\Delta E_m = 0$ corresponding to $|m\rangle = |0\rangle$. Thus we obtain

$$\lim_{T\to\infty} \langle O_2(t)O_1(0)\rangle = \sum_n \langle 0|\hat{O}_2|n\rangle\langle n|\hat{O}_1|0\rangle e^{-M_n t} \tag{3.12}$$

In large distance the term which has the lowest M_n dominates. Consequently the correlator decays as

$$\langle O_2(t)O_1(0)\rangle \sim \exp(-M_1 t). \tag{3.13}$$

Analogous to the high temperature expansion in statistical mechanics, one can use strong coupling expansion in lattice gauge theory for small lattice coupling β (large g^2). In this method one merely expands the Boltzman factor $\exp(-S[U])$ in powers of β, to determine the expectation values of observable on the lattice. Let us first consider the expectation value of a rectangular Wilson loop traversed in a clockwise direction on the lattice. Following the group integral identity

$$\int_{SU(3)} dU\ U_{ab} = 0, \tag{3.14}$$

the contribution to the expectation value from the first term of the expansion is zero. Non vanishing contributions comes from the higher order terms of the expansion. The first non-vanishing contribution comes from the term with plaquettes oriented in counter clockwise direction filling the Wilson loop since

$$\int_{SU(3)} dU\ U_{ab}U_{cd} = 0, \tag{3.15}$$

$$\int_{SU(3)} dU\ U_{ab}U^{\dagger}_{cd} = \frac{1}{3}\delta_{ad}\delta_{bc}. \tag{3.16}$$

The higher order contribution to the expectation value comes from the bumps of plaquettes on the tiling surface filling the Wilson loops. Following this method one can easily find the Wilson loop expectation value, in the strong coupling limit to be

$$\langle W_c\rangle = 3\left(\frac{\beta}{18}\right)^{n_A}(1 + \mathcal{O}(\beta)) \tag{3.17}$$

where n_A is the number of the plaquettes filling the Wilson loop. Following a similar technique the connected correlators of Wilson loop operators can be easily calculated for large lattice couplings. For the plaquette-plaquette correlator relevant diagrams for the strong coupling expansion consists of tubes of plaquettes. The leading order strong

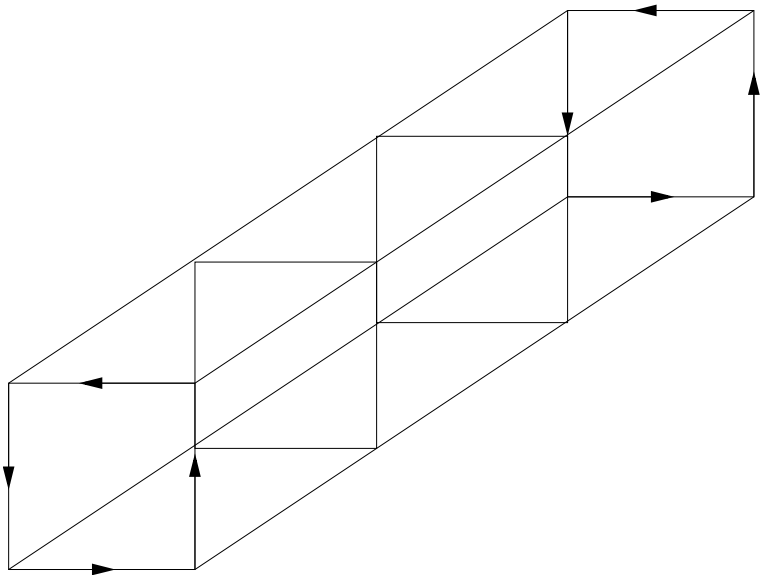

Figure 3.1: Leading order diagram for strong coupling expansion of the plaquette-plaquette correlator.

coupling diagram is shown in Fig. 3.1, where the tube connecting the source and sink plaquettes is tiled with fundamental plaquettes. From this diagram one can easily find that in the leading order the plaquette-plaquette connected correlator behaves as,

$$C(\Delta t) \sim \left(\frac{\beta}{6}\right)^{4n_t}, \tag{3.18}$$

where $\Delta t = an_t$ is the temporal separations between the two plaquettes. So the glueball mass from the strong coupling expansion can be obtained as,

$$m_g \sim -4 \ln\left(\frac{\beta}{6}\right)(1 + \mathcal{O}(\beta)). \tag{3.19}$$

The higher order contribution comes from the deformations on the surface of the tube of plaquettes connecting the source and sink plaquettes.

3.2 Glueball Operator Methodology

We have seen in the last section that the spectrum of glueballs can be extracted from (3.13) using correlators of certain operators. In this section we will discuss methods for choosing glueball operators. In the continuum limit, unitary irreducible representation of the rotation group $SO(3)$ characterizes the spin of a bosonic state. In lattice discretization, rotation symmetry is broken down to the symmetry group of the cube. In

the continuum limit rotation invariance is expected to be restored and the eigenstates of the transfer matrix can be classified according to the irreducible representations of the $3d$ rotation group.

3.2.1 The symmetry group of the cube

The symmetry group of a cube is the cubic or octahedral group **O**, an exact symmetry group for theory on lattice. The rotation around an uniquely determined symmetry axis of a cube can be identified with non-identity elements of the cubic group **O**. The number of different rotations which can be performed around the axes, defines it's order. We fix our notation by means of Fig. 3.2.

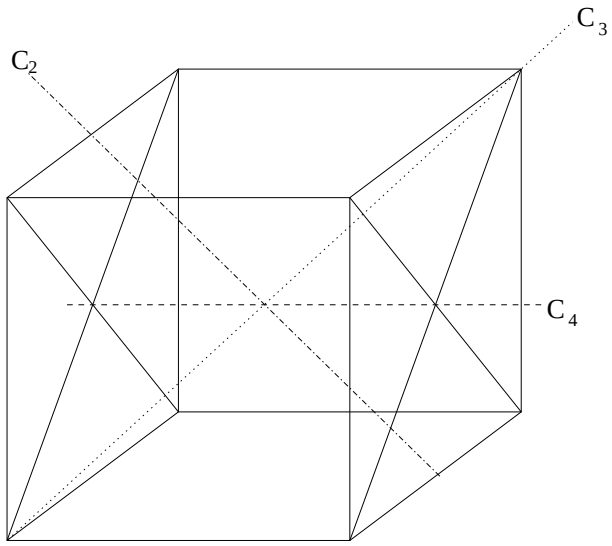

Figure 3.2: Symmetry axes of rotations for the group $\mathbf{O_h}$.

If a rotation by an angle $\phi = \frac{2\pi}{n}$ (n integer) makes a cube coincident with itself, then the rotation axis is known as n-fold axis or axis of order n. There are three 4-fold axes, four 3-fold axes and six 2-fold axes for the cube. Including the identity (n=1) there are 24 elements altogether. The group elements are divided in five conjugacy classes $E = \{E\}$, $C_4 = \{C_4^{(i)}, (C_4^{(i)^3})\}$ (with $i = 1, 2, 3$), $C_4^2 = \{(C_4^{(i)})^2\}$ (with $i = 1, 2, 3.$), $C_3 = \{C_3^{(i)}, (C_3^{(i)})^2\}$ (with $i = 1, ..., 4$) and $C_2 = C_2^{(i)}$ (with $i = 1, ..., 6$). Hence there are five inequivalent irreducible representations $A_1(1), A_2(1), E(2), T_1(3)$ and $T_2(3)$. The quantities in the parenthesis are dimensions of the irreducible representations satisfying

$$\sum_{\mu} n_{\mu}^2 = dim(G) \tag{3.20}$$

where n_μ is the dimension of the irreducible representation μ and $dim(G)$ is the order of the group G. The character table for these irreducible representations is given in table 3.1.

R	E	$C_2(6)$	$C_3(8)$	$C_4(6)$	$C_4^2(3)$
A_1	1	1	1	1	1
A_2	1	-1	1	-1	1
E	2	0	-1	0	2
T_1	3	-1	0	1	-1
T_2	3	1	0	-1	-1

Table 3.1: Character table for different conjugacy classes.

There are two discrete symmetries in addition to the transformation of the cubic group. They are total space reflection and charge conjugation. The eigenvalues of the space reflection are the parity $P = \pm 1$. The direct product of the octahedral and parity forms 48 elements group $\mathbf{O_h} = \mathbf{O} \otimes \mathbf{Z_2}$ whose representations are labelled by R^P. The charge conjugation is equivalent to the complex conjugation of Wilson loops. The eigenvalues of the charge conjugation are C-parity $C = \pm 1$. The states belonging to an irreducible representation of the lattice symmetry group are therefore labelled by R^{PC}.

3.2.2 Spin on the Lattice

In this section we will construct irreducible representations of the symmetry group of the cube on Wilson loop operators and hence will explain the relationship between those representations and the spin states in the continuum limit for lattice gauge theory.

In the continuum limit of lattice gauge theory rotation invariance is expected to be restored. Let D_J be the irreducible representation in the continuum limit for spin J and denote the corresponding states by $|\psi\rangle_J$ ($\beta = \infty$) [5] for integer spin $J = 0, 1, \ldots$. For all finite values of β i.e., for finite lattice spacing the irreducible representations of the symmetry group of the lattice are $R = A_1, A_2, E, T_1, T_2$ and let the corresponding states be $|\psi\rangle_R$. In the continuum limit these states can be expanded in terms of spin

R	A_1	A_2	E	T_1	T_2
J	0	3	2	1	2

Table 3.2: Lowest spin content for the irreducible representation of **O**

states

$$|\psi\rangle_R = \sum_{J,m} c^R_{J,m} |\psi\rangle_{J,m}. \tag{3.21}$$

Spin J can only contribute to the right hand side of (3.21) if $D^{\mathbf{O}}_J \supset R$. Where $D^{\mathbf{O}}_J$ is the subduced representation [6] of D_J, which is obtained by embedding the cubic group **O** into the rotation group $SO(3)$. Up to $J = 4$ one finds

$$D^{\mathbf{O}}_0 = A_1, \tag{3.22}$$

$$D^{\mathbf{O}}_1 = T_1, \tag{3.23}$$

$$D^{\mathbf{O}}_2 = E \oplus T_2, \tag{3.24}$$

$$D^{\mathbf{O}}_3 = A_2 \oplus T_1 \oplus T_2, \tag{3.25}$$

$$D^{\mathbf{O}}_4 = A_1 \oplus E \oplus T_1 \oplus T_2. \tag{3.26}$$

Let O_R be a lattice operator which transform under irreducible representation R. An application of O_R on the vacuum creates a state which is a superposition of various eigenstates of the Hamiltonian

$$\psi_R = \sum_\alpha c^R_\alpha \psi_\alpha \tag{3.27}$$

In the continuum limit, the states ψ_α belong to spin J multiplets. In this sense ψ_R contains various spin states. Spin J states can occur in right hand side of (3.21) only if $D^{\mathbf{O}}_J \supset R$. The representation of the cubic group and their lowest spin content are given in table (3.2).

3.2.3 Irreducible representations of O_h on Wilson loops

A representation of the group G can be obtained by applying the transformation of the group G on any function ψ [7]. Then either the function ψ can be expressed linearly in terms of base functions or ψ itself can be a base function. This statement remains true if we split the representation into its irreducible constituents. So any function ψ is expressible as a sum of functions which can act as base functions in the various irreducible representation

$$\psi = \sum_\nu \sum_{i=1}^{d_\nu} \psi^{(\nu)}_i. \tag{3.28}$$

Consider a set of functions $\left(\psi_1^{(\nu)}, \psi_2^{(\nu)}, ..., \psi_{d_\nu}^{(\nu)}\right)$ that form a d_ν dimensional basis for irreducible representation $D^{(\nu)}$. The effect of any symmetry operation on a basis function can be represented as

$$R\psi_i^{(\nu)} = \sum_j \psi_j^{(\nu)} D_{ji}^{(\nu)}(R). \tag{3.29}$$

The function $\psi_i^{(\nu)}$ belongs to i th row of the ν th irreducible representation. Multiplying both side of (3.29) by $D_{lm}^{(\mu)*}$ and taking the sum over group elements we get

$$\sum_R D_{lm}^{(\mu)*}(R) R\psi_i^{(\nu)} = \sum_j \psi_j^{(\nu)} \sum_R D_{lm}^{(\mu)*}(R) D_{ji}^{(\nu)}(R) \tag{3.30}$$

$$= \frac{g}{d_\nu} \sum_j \psi_j^{(\nu)} \delta_{lj}\delta_{mi}\delta_{\mu\nu} = \frac{g}{d_\nu}\psi_l^{(\nu)}\delta_{mi}\delta_{\mu\nu} \tag{3.31}$$

where g is the order of the group. In particular for $l = m$ we can write

$$\sum_R D_{ll}^{(\mu)*}(R) R\psi_i^{(\nu)} = \frac{g}{d_\nu}\psi_l^{(\nu)}\delta_{li}\delta_{\mu\nu} \tag{3.32}$$

In eq. (3.32) and for the rest of this chapter we drop the summation convention. Let us define a projection operator

$$P_i^{(\mu)} = \frac{d_\mu}{g}\sum_i D_{ii}^{(\mu)*}(R) R. \tag{3.33}$$

Thus the effect of projection operator on a basis function

$$P_i^{(\mu)}\psi_j^{(\nu)} = \psi_i^{(\mu)}\delta_{\mu\nu}\delta_{ij}. \tag{3.34}$$

Applying the operator $P_i^{(\mu)}$ on (3.28), we obtain the result

$$\psi_i{}^{(\mu)} = \frac{d_\mu}{g}\sum_R D_{ii}^{(\mu)*}(R) R\psi. \tag{3.35}$$

In analogy to the above, we can write a function $\psi^{(\nu)}$ belonging to the νth irreps. as a sum of functions belonging to the various rows of that representation i.e.,

$$\psi^{(\nu)} = \sum_{i=1}^{d_\nu} \psi_i^{(\nu)}. \tag{3.36}$$

Now taking sum over i in Eq. (3.35) we get

$$\psi^{(\mu)} = \frac{d_\mu}{g} \sum_R \chi^{(\mu)*}(R) R\psi. \tag{3.37}$$

Thus

$$\psi^{(\mu)} = P^{(\mu)}\psi. \tag{3.38}$$

On lattices the arbitrary function ψ is replaced by Wilson loops. In the following, we will define wilson loop of length L by L-tuple $\left(\hat{f}_1, \hat{f}_2, ..., \hat{f}_L\right)$ with $\sum_{i=1}^{L} f_i = 0$, where $\hat{f}_i \in \{\pm\hat{e_j} | j = 1, 2, 3\}$, e_j being unit vectors corresponding to the space like co-ordinates of our lattice. The L-tuples which are identical upto cyclic permutations are known as equivalent. The equivalence class corresponding to $\left(\hat{f}_1, \hat{f}_2, ..., \hat{f}_L\right)$ is denoted by $[\hat{f}_1, \hat{f}_2, ..., \hat{f}_L]$.

Since, under C-parity the gauge field A_μ transforms as

$$A_\mu \rightarrow^C -A_\mu^T \tag{3.39}$$

It follows that the real part of the Wilson loop operators have C-parity $C = +1$ and the imaginary parts have C-parity $C = -1$. So, the C-parity on the Wilson loops in terms of the L tuple can be defined as

$$C[\hat{f}_1, \hat{f}_2, ..., \hat{f}_L] = [-\hat{f}_L, -\hat{f_{L-1}}, ..., -\hat{f}_1] \tag{3.40}$$

Operators with definite C-parity $C = \pm 1$ is defined as the combination

$$[\hat{f}_1, \hat{f}_2, ..., \hat{f}_L]_\pm = \frac{[\hat{f}_1, \hat{f}_2, ..., \hat{f}_L] \pm [-\hat{f}_L, -\hat{f_{L-1}}, ..., -\hat{f}_1]}{2} \tag{3.41}$$

the parity operation on the operators are defined as

$$P[\hat{f}_1, \hat{f}_2, ..., \hat{f}_L] = [-\hat{f}_1, -\hat{f}_2, ..., -\hat{f}_L] \tag{3.42}$$

and the operators with defined parity $P = \pm 1$ are

$$[\hat{f}_1, \hat{f}_2, ..., \hat{f}_L]^{\pm} = \frac{[\hat{f}_1, \hat{f}_2, ..., \hat{f}_L] \pm [-\hat{f}_1, -\hat{f}_2, ..., -\hat{f}_L]}{2} \tag{3.43}$$

Symmetry operations on the loops are represented as

$$\mathcal{R}[\hat{f}_1, \hat{f}_2, ..., \hat{f}_L] = [\mathcal{M}_g \hat{f}_1, \mathcal{M}_g \hat{f}_2, ..., \mathcal{M}_g \hat{f}_L] \tag{3.44}$$

for $g \in O_h$ and $\mathcal{M}_g$ being the three dimensional rotation matrix corresponding to group element g in vector representation on the basis $\hat{e}_i$ $(i = 1, 2, 3)$.

Alternatively one can use following protocol [9] for the loops on the lattice

Index	Name	Prototype path	No. of links (l_s, l_t)
1	S-Plaquette	[X,Y,-X,-Y]	(4,0)
2	S-Rectangle	[X,X,Y,-X,-X,-Y]	(6,0)
3	T-Plaquette	[X,T,-X,T]	(2,2)
4	T-Rectangle	[X,X,T,-X,-X,-T]	(4,2)
5	S-Chair	[X,Y,-X,Z,-Y,-Z]	(6,0)
6	S-Butterfly	[X,Y,-X,Y,Z,-Y,-Z,Y]	(8,0)
7	S-Sunbed	[X,X,Y,-X,-X,Z,-Y,-Z]	(8,0)
8	T-Chair	[X,T,-X,Z,-T,-Z]	(4,2)
9	T-Sunbed	[X,X,T,-X,-X,Z,-T,-Z]	(6,2)
10	Knot	[X,T,-X,-T,Z,-Y,-Z,Y]	(6,2)
11	LS-Knot	[X,T,-X,-T,Z,Z,-Y,-Z,-Z,Y]	(8,2)
12	LT-Knot	[X,X,T,-X,-X,-T,Z,-Y,-Z,Y]	(8,2)

Table 3.3: Wilson loop prototype

The 24 symmetric operations on those loops are described in table 3.4

Index	Operations	Index	Operations
1	$(x,y,z) \to (x,y,z)$	13	$(x,y,z) \to (-z,y,x)$
2	$(x,y,z) \to (-z,-y,-x)$	14	$(x,y,z) \to (-x,-y,z)$
3	$(x,y,z) \to (z,x,y)$	15	$(x,y,z) \to (-y,x,z)$
4	$(x,y,z) \to (-y,-x,-z)$	16	$(x,y,z) \to (-z,-x,y)$
5	$(x,y,z) \to (y,z,x)$	17	$(x,y,z) \to (-x,z,y)$
6	$(x,y,z) \to (-x,-z,-y)$	18	$(x,y,z) \to (-y,-z,x)$
7	$(x,y,z) \to (z,y,-x)$	19	$(x,y,z) \to (-x,y,-z)$
8	$(x,y,z) \to (x,-y,-z)$	20	$(x,y,z) \to (z,-y,x)$
9	$(x,y,z) \to (y,x,-z)$	21	$(x,y,z) \to (-z,x,-y)$
10	$(x,y,z) \to (z,-x,-y)$	22	$(x,y,z) \to (y,-x,z)$
11	$(x,y,z) \to (x,z,-y)$	23	$(x,y,z) \to (-y,z,-x)$
12	$(x,y,z) \to (y,-z,-x)$	24	$(x,y,z) \to (x,-z,y)$

Table 3.4: Symmetry operations on Wilson loops.

Using symmetry operations on any Wilson loop from table 3.4 and characters of the irreps from table 3.1 one can easily construct operators for all the symmetry channels.

In our calculation we used only square wilson loops to construct glueball operators. Using square wilson loops, glueball operators for the scalar and tensor channel can be constructed in following way

$$\mathcal{A} = Re(\mathcal{P}_{xy} + \mathcal{P}_{xz} + \mathcal{P}_{yz}) \tag{3.45}$$

$$\mathcal{E}_1 = Re(\mathcal{P}_{xz} - \mathcal{P}_{yz}), \quad \mathcal{E}_2 = Re(\mathcal{P}_{xz} + \mathcal{P}_{yz} - 2\mathcal{P}_{xy}), \tag{3.46}$$

where $\mathcal{P}_{ab}$ is the square Wilson loop in plane $ab \in x, y, z$. $\mathcal{A}$ is the glueball operator for the scalar channel, while $\mathcal{E}_1$ and $\mathcal{E}_2$ are the glueball operators for the tensor channel.

Bibliography

[1] K. G. Wilson,*Phys. Rev.* **D10** (1974) 2445.

[2] M. Creutz, *Phys. Rev. D* **15** (1970) 1128.

[3] M. Lüscher, *Comm. Math. Phys.* **54** 283.

[4] K. Osterwalder, E. Seiler, *An. Phys.* **110** (1978) 440.

[5] B. Berg, A. Billoire, *Nucl. Phys.* **B 221** (1983) 109-140.

[6] S. L. Altman, A. P. Cracknell, *Rev. Mod. Phys.* **37** (1965) 19.

[7] M. Hamermesh, *Group theory and its application to physical problems*, (Addison-Wesley, Reading, Massachusetts).

[8] C. Gattringer, C. B. Lang, *"Quantum Chromodynamics on the Lattice"*, (Springer, Berlin Heidelberg 2010).

[9] Y. Chen *et. al.*, *Phys. Rev.* **D73** (2006) 014516 `[arXiv:hep-lat/0510074]`.

Chapter 4

Algorithm

The vacuum expectation value of an observable in quantized lattice gauge theory can be obtained using following ensemble average

$$\langle O \rangle = \frac{\int DU O[U] \exp(-S[U])}{\int DU \exp(-S[U])} \tag{4.1}$$

Analytical computation of this ensemble average on lattice is practically impossible as it poses a problem of performing tremendously large number of integrals for a considerable lattice volume.

The ensemble average $\langle O \rangle$ in eq.(4.1) can be efficiently computed by generating a sequence of link variable configurations with a probability distribution given by the Boltzman factor $\exp(-S[U])$. The ensemble average can be given approximately by

$$\langle O \rangle \approx \frac{1}{N} \sum_{n=1}^{N} O[U_n] \tag{4.2}$$

where U_n sampled according to the probability distribution

$$dP(U) = \frac{\exp(-S[U])}{\int DU \exp(-S[U])} \tag{4.3}$$

which is known as the Gibbs measure. We approximate the integral by N gauge configurations $\{U_n\}$. The exact expectation value of the observable can be obtained in the limit $N \to \infty$.

The main task for simulating pure $SU(3)$ gauge theory on lattice is to generate configurations $\{U_n\}$ according to probability distribution given by (4.3). The standard procedure for simulating gauge fields is to generate a stochastic sequence of configurations following an equilibrium distribution $P(U)$ starting from an arbitrary configuration. This method is known as Markov process where the Markov chain configurations U_n are generated subsequently

$$U_0 \to U_1 \to U_2 \to ... \tag{4.4}$$

The index n for a field configuration represents the sequential order in which it is generated. This index are often referred to as computation time. Update to a new configuration from an existing one is known as a Monte Carlo step.

In the Markov process the transition probability from the configuration U_{n-1} to the configuration U_n is denoted by

$$T(U_n = U'|U_{n-1} = U) \equiv T(U'|U) \tag{4.5}$$

The transition probability depends only on the configuration U_{n-1} and the configuration U_n but is independent of the initial value of the index. The probability of any configuration U_n is represented by $P(U_n)$ and the criterion followed by any probability distribution are the following

(i) $P(U) > 0$ for all U

(ii) $\sum_U P(U) = 1$.

The transition probability for the Markov process obeys following requirements

(i)$T(U'|U) \geqslant 0$ for all U, U'

(ii)$\sum_{U'} T(U'|U) = 1$ for all U.

The probability to hop into a configuration U' at any step is equal to the probability to hop out of U' in a Markov process. The corresponding balance equation is the following

$$\sum_U T(U'|U)P(U) = \sum_U T(U|U')P(U') \tag{4.6}$$

where the left hand side represents the total probability to hop into the configuration U' and the right hand side represents the total probability to hop out of U'. Using the normalization property the sum on the right hand side of (4.6) can be written as

$$\sum_U T(U'|U)P(U) = P(U') \tag{4.7}$$

This equation implies that the equilibrium distribution $P(U)$ is a fixed point of the Markov process. Applying the transition matrix repeatedly on an arbitrary gauge configuration U_0 with occurence probability $P^{(0)}(U)$ one obtains the equilibrium configuration U distributed according to $P(U)$.

$$P^{(0)} \to P^{(1)} \to P^{(2)} \to ... \to P \ \ (= \text{equilibrium distribution}) \tag{4.8}$$

The strong ergodicity of a Markov process can be obtained when all the configurations of the Markov chain are accessible, which can be obtained for strictly positive transition matrix elements $T(U'|U)$ for all pairs of U and U'. A solution of the balance eqn(4.6) can be obtained when equality holds for each term

$$T(U'|U)P(U) = T(U|U')P(U') \tag{4.9}$$

This equality is known as the detailed balance condition. Most Monte Carlo algorithms follow the detailed balance condition.

4.1 Metropolis Algorithm

The metropolis algorithm was originally proposed by Metropolis *et al.* [1]. It advances the Markov chain from from an initial configuration U_{n-1} to a new configuration U_n. One applies the Metropolis algorithm to update a given configuration using the following steps

(i) Use some a-priori transition probability $T_0(U'|U)$ to choose some candidate configuration U'.

(ii) Accept the candidate configuration U' with acceptance probability

$$T_A(U'|U) = \min\left(1, \frac{T_0(U|U')\exp(-S[U'])}{T_0(U'|U)\exp(-S[U])}\right) \tag{4.10}$$

when the selected configuration U' is not accepted, the old configuration U is considered again in the Markov chain.

(iii) Repeat the steps (i) and (ii).

The total transition probability $T = T_0 T_A$ satisfies the detailed balance condition. For the symmetric selection probability

$$T_0(U|U') = T_0(U'|U) \tag{4.11}$$

(4.10) simplifies to

$$T_A(U'|U) = \min\left(1, \exp(-\Delta S)\right) \quad \text{with} \quad \Delta S = S[U'] - S[U]. \tag{4.12}$$

So the new configuration is always accepted when the action gets lowered for new configuration and accepted with probability $\exp(-\Delta S)$ when the action increased by ΔS.

4.2 Metropolis Algorithm for Wilson Gauge Action

The locality property of the Wilson gauge action makes it convenient to use Metropolis algorithm for Wilson's gauge action. Calculation of action difference ΔS in (4.12) involves a single link variable $U_\mu(n)$. As a result of that, the computer time required per link update is quite small. The candidate configuration U' for the Metropolis update differs from the configuration U by the value of single link variable $U_\mu(n)$. In four dimensions this link $U'_\mu(n)$ is shared by six plaquettes, which are affected when changing $U_\mu(n) \to U'_\mu(n)$. Using this locality the change in the action ΔS can be written as

$$\Delta S = -\frac{\beta}{N} Re\ tr[(U'_\mu(n) - U_\mu(n))A], \tag{4.13}$$

where

$$\begin{aligned} A = \sum_{i=1}^{6} P_i = \sum_{\nu \neq \mu} & (U_\nu(n+\hat{\mu}) U^\dagger_\mu(n+\hat{\nu}) U^\dagger_\nu(n) \\ & + U^\dagger_\nu(n+\hat{\mu}-\hat{\nu}) U^\dagger_\mu(n-\hat{\nu}) U_\nu(n-\hat{\nu})) \end{aligned} \tag{4.14}$$

and N corresponds to the $SU(N)$ gauge theory under consideration. Here β is known as the inverse lattice coupling which is related to the coupling g^2 of eq. 2.21 by $\beta = \frac{2N}{g^2}$.

The products P_i of the link variables of the plaquettes are known as staples. A represents the sum of all staples for a link variable, which are affected by the change of $U_\mu(n)$.

One should choose the candidate $SU(N)$ link variables $U'_\mu(n)$ in such a way that it is not too far from old link variable $U_\mu(n)$ so that and the average acceptance probability for $U'_\mu(n)$ does not become too small. One possibility is to take product of a random $SU(N)$ matrix X in vicinity of 1 with the old link $U_\mu(n)$

$$U'_\mu(n) = X \cdot U_\mu(n) \tag{4.15}$$

Construction of the matrices X is discussed in next section. The Metropolis algorithm for $SU(N)$ gauge theory can be described in following steps:

(i) Given a starting configuration choose a candidate link variable $U'_\mu(n)$ according to some selection probability T_0.

(ii) Compute the change in action ΔS using the sum of staples. Accept the new variable $U'_\mu(n)$ when $\exp(-\Delta S) \geqslant r$ and reject otherwise. Where r is random number distributed uniformly in the interval $[0, 1)$.

(iii) Repeat these steps from beginning for all the lattice sites n and directions μ.

In step 2 the candidate link is always accepted with decreased action in addition due to the random number r the configurations with increased action is also accepted randomly. This feature reproduces quantum fluctuations of the system.

4.3 Heat Bath Algorithm

In the last section we discussed the single link Metropolis update algorithm. In this section we will describe a more efficient algorithm namely the heat bath algorithm.

In the heat bath method the first two steps of the single link Metropolis update are combined into a single step and the new link variable $U'_\mu(n)$ is chosen according to the local probability distribution

$$dP(U) = dU \exp\left(\frac{\beta}{N} Re\ tr[UA]\right) \tag{4.16}$$

where A is the sum of staples calculated according to (4.14). In this algorithm all the links except for $U = U_\mu(n)$, are held fixed when updating a link at site n and in μ direction. dU denotes the Haar measure for the gauge group. The heat bath algorithm is not directly applicable for updating $SU(3)$ link variables, however one can use a pseudo heat bath algorithm by updating $SU(2)$ subgroups of $SU(3)$.

By updating two different $SU(2)$ subgroups of $SU(3)$ in turn, one can cover the whole of $SU(3)$. However for efficiency reasons, it is better to update all the three different $SU(2)$ subgroups of $SU(3)$. This procedure can be generalized to $SU(N)$ where $SU(N)$ is updated by updating N-different $SU(2)$ subgroups of $SU(N)$.

To update a $SU(2)$ matrix we use the property that the sum of $SU(2)$ matrices is proportional to another $SU(2)$ matrix. Let us construct an $SU(2)$ matrix $V = \frac{A}{\sqrt{det[A]}}$. Where $det[A] \geqslant 0$. If $det[A] = 0$ one chooses a random $SU(2)$ matrix for U. The probability distribution (4.16) can now be written as

$$dP(U) = dU \exp\left(\frac{1}{2} a\beta Re\ tr[UV]\right). \tag{4.17}$$

Where $a = \sqrt{det[A]}$. Let us define a matrix X by the product $X = UV$. Since the Haar measure is invariant under gauge transformation we can write the local probability distribution of X as

$$dP(X) = dX \exp\left(\frac{1}{2} a\beta Re\ tr[X]\right). \tag{4.18}$$

The candidate link can be obtained from the matrix X distributed according to (4.18)

$$U'_\mu(n) = U = XV^\dagger = X\frac{A^\dagger}{\sqrt{det[A]}}. \tag{4.19}$$

We use the following representation for the $SU(2)$ matrix X

$$X = x_0 + i\mathbf{x} \cdot \sigma \tag{4.20}$$

where σ denotes the vector of three Pauli matrices and

$$det[X] = x_0^2 + |\mathbf{x}|^2 = 1. \tag{4.21}$$

Using this representation one can write the distribution for X in the form

$$dP(X) \propto\ dx_0 \sqrt{1 - x_0^2}\ d^3n\ \delta(n^2 - 1)\ \exp(a\beta x_0) \tag{4.22}$$

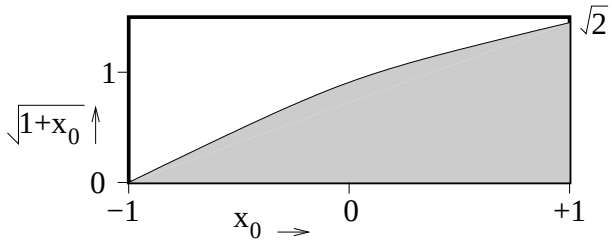

Figure 4.1: Distribution of x_0.

with $d^3n\ \delta(n^2-1) \equiv d^2\Omega$ and $x_i = \sqrt{1-x_0^2}\ n_i$. Determination of the $SU(2)$ matrices according to (4.18) is now reduced to generation of a random variable x_0 with probability $P(x_0) \propto e^{a\beta x_0}$ and generation of a unit vector n_i for $i = 1, 2, 3$ such that $n^2 = 1$.

Fabricius & Haan [3] and Kennedy & Pendleton [2] observed that if one generates

$$P'(x_0) \propto e^{a\beta x_0}\sqrt{1-x_0}\,\theta(1-x_0) \tag{4.23}$$

then one would have to correct only for $\sqrt{1+x_0}\,\theta(1+x_0)$. This correction is implemented by an accept/reject test. If u_2 is a flat random number between $[0,1)$, then accept x_0 if $2u_2^2 \leq 1+x_0$. $\sqrt{1+x_0}$ varies from 0 to $\sqrt{2}$. So our random variable is normalized to $\sqrt{2}$. s_0 is accepted if the random variable is below the curve (shaded area). The shaded area is the region $\sqrt{2} \leq \sqrt{1+x_0}$.

For $SU(3)$, one can construct updating matrices X from $SU(2)$ matrices embedded in 3×3 matrices according to

$$R = \begin{pmatrix} r_{11} & r_{12} & 0 \\ r_{21} & r_{22} & 0 \\ 0 & 0 & 1 \end{pmatrix},\ S = \begin{pmatrix} s_{11} & 0 & s_{12} \\ 0 & 1 & 0 \\ s_{21} & 0 & s_{22} \end{pmatrix},\ T = \begin{pmatrix} 1 & 0 & 0 \\ 0 & t_{11} & t_{12} \\ 0 & t_{21} & t_{22} \end{pmatrix} \tag{4.24}$$

This pseudo heat bath update for the $SU(2)$ subgroups may also be combined with overrelaxation steps as discussed in the next section.

4.4 Overrelaxation Algorithm

Overrelaxation algorithm [4] replaces each link on the lattice with another group element ($SU(3)$ in our case) in such a way that the action remains the same but the new link is as far as possible in the group space from the original element. To perform the overrelaxation method one uses the fact that in the Metropolis algorithm new configurations are always accepted if they do not change the action. The starting point is the

probability distribution (4.16) of a single link variable $U_\mu(n) = U$, in the background of its neighbors which we hold fixed, with the sum of staples A calculated according to (4.14). The matrix A can be decomposed as:

$$A = A\frac{1}{(A^\dagger A)^{1/2}}(A^\dagger A)^{1/2} \equiv \ O(A^\dagger A)^{1/2} \ \equiv \ OH \tag{4.25}$$

where H is a hermitian matrix. The $U(3)$ matrix O can be reduced to $SU(3)$ matrix by multiplying with matrix $I(\alpha)$ proportional to identity matrix with $det[I(\alpha)] = det[O^\dagger]$. Therefore,

$$A = \tilde{O}I^\dagger(\alpha)H \tag{4.26}$$

where $\tilde{O} = OI(\alpha)$ is a $SU(3)$ matrix. Diagonalising the matrix H by the unitary matrix V,

$$H = V^\dagger DV \tag{4.27}$$

we obtain

$$tr[UA] = tr[VU\tilde{O}V^\dagger I^\dagger(\alpha)D] \equiv tr[U'I^\dagger(\alpha)D] \tag{4.28}$$

The action depends upon the diagonal elements of U' only and the non-diagonal elements of U' can be suitably reflected. Indeed, the measure and the exponential are invariant under three reflections of non-diagonal elements. Reflections of the non-diagonal elements of U are represented as.

Reflection (1)

$$U^r_{12} = -U_{12}, U^r_{21} = -U_{21}, \tag{4.29}$$
$$U^r_{13} = -U_{13}, U^r_{31} = -U_{31} \tag{4.30}$$

Reflection (2)

$$U^r_{12} = -U_{12}, U^r_{21} = -U_{21}, \tag{4.31}$$
$$U^r_{23} = -U_{23}, U^r_{32} = -U_{32} \tag{4.32}$$

Reflection (3)

$$U^r_{23} = -U_{23}, U^r_{32} = -U_{32}, \tag{4.33}$$
$$U^r_{13} = -U_{13}, U^r_{31} = -U_{31} \tag{4.34}$$

The reflection operations leads to a new group element having the same energy as the original one. The reflected link finally reads,

$$U_R = V^\dagger [VOUV^\dagger]_r VO^\dagger \tag{4.35}$$

where the subscript r implies that the reflection operation applied to the matrix in the bracket. The overrelaxation algorithm alone is not ergodic. It samples the configuration space on the subspace of constant action. This is called the microcanonical ensemble. Since one wants to determine configurations according to the canonical ensemble, i.e., distributed according to the Boltzmann weight, one has to combine the overrelaxation steps with other updating algorithms, in our case we combined overrelaxation with the heat bath algorithm.

4.5 Initialisation

To start the simulation one can choose any field configuration. After sufficient computer time, configurations distributed according to the equilibrium distribution will be produced due to the Markov chain property (4.8). The cold start and the hot start are two typical starting configurations.

In cold start all the link variables are set as 3×3 unit matrices ($U_\mu = 1$). This configuration corresponds to minimal action, situation approximately expected for small g (large β). The weak coupling regime corresponds to low temperature of corresponding statistical system, hence the name.

In hot start random matrices are chosen as starting configuration. One can also start with mixed configuration, where one half of the field variables are chosen cold and the other half are chosen hot.

The equilibrium distribution can be obtained after a certain number of sweeps through the lattice. A sweep through the lattice is referred to visiting all the links at least once. One determines the sufficient number of equilibriation sweeps for any observable by studying that observable started with cold and hot starts separately. For example we look at the value of the bare plaquette at $\beta = 6.1$ in fig. 4.2. As soon as the curves for the observables from the hot and the cold start approach each other, the system is nearing equilibrium. In general the number of sweeps required to obtain the equilibrium distribution depends on the updating algorithm, the type of action used, the lattice gauge coupling β, and the size of the lattice.

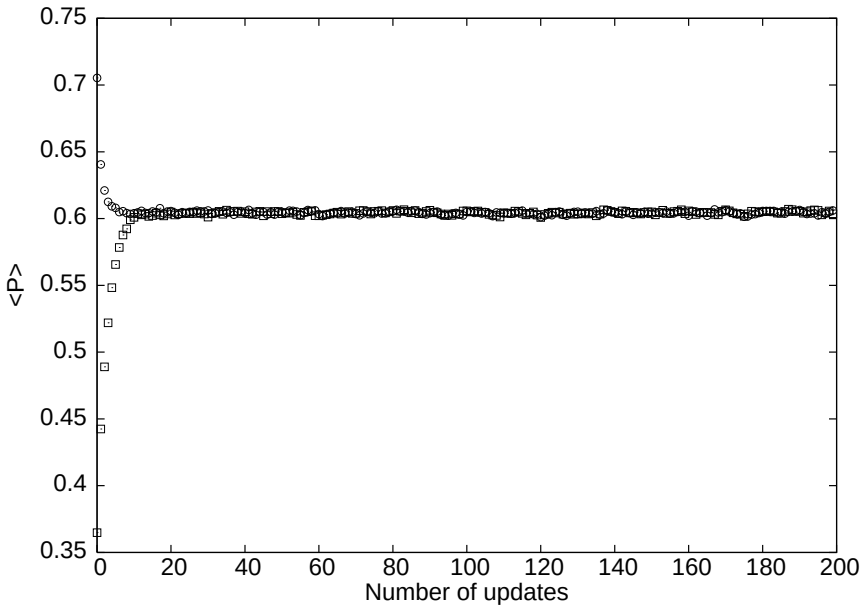

Figure 4.2: The bare plaquette measured at $\beta = 6.10$ starting with hot and cold start. The data points with circles are obtained from cold start and the boxes are obtained from hot start.

4.6 Statistical Analysis of Data

Monte Carlo simulations generate configuration samples $[U_n], (n = 1, 2, ..., N)$ for a Markov sequence. This allows one to determine different observables $A[U]$. An estimator for the expectation values of those observables is given by the sample average $\overline{A}$. Averaging over infinitely large number of sample gives the ensemble average equal to the expectation value $\overline{\overline{A}} = \langle A \rangle$. In ideal case where the configurations in each sample are uncorrelated, the sample average $\overline{A}$ is normally distributed around $\overline{\overline{A}}$ with variance

$$\sigma^2_{\overline{A}} = \frac{1}{N-1}(\overline{A^2} - \overline{A}^2) \tag{4.36}$$

In this case the error on the sample average is quoted as,

$$\overline{\overline{A}} = \overline{A} \pm \sigma_{\overline{A}}. \tag{4.37}$$

In Monte Carlo simulations the data sample is the result of a (computer-)time series and in most of cases the generated configurations are in fact correlated. As a result the observables are not statistically independent. The correlation in the sequence of the generated configurations is known as autocorrelation. The autocorrelation function for the observable A is defined as,

$$C_A(t) = \langle (A_i - \langle A_i \rangle)(A_{i+t} - \langle A_{i+t} \rangle) \rangle. \tag{4.38}$$

In a typical situation the normalized autocorrelation function $\Gamma_A(t)$ for the observable A exhibits exponential behaviour for asymptotically large t:

$$\Gamma_A(t) \equiv \frac{\Gamma_A(t)}{\Gamma_A(0)} \sim \exp\left(-\frac{t}{\tau_{A,exp}}\right), \tag{4.39}$$

and $\tau_{A,exp}$ is known as the exponential autocorrelation time for the observable A. And the integrated autocorrelation time is defined as

$$\tau_{A,int} = \frac{1}{2} + \sum_{t=1}^{N} \Gamma_A(t). \tag{4.40}$$

One can obtain corrected error estimates from an updating sequence with autocorrelations using binning analysis. For a long enough sequence of configurations one can build blocks of subsequent observables, called bins, and average the observables first in the bins. The obtained bin averages themselves can then be considered as results of single measurements, and can be used to estimate the variance according to (4.36). If the bin sizes are larger than the autocorrelation time, then the average values in the bins are practically uncorrelated, and the obtained error estimate is unbiased.

One can use the jackknife analysis [5] when a long enough sequence of configurations is not available. Consider a not very large sample of independent measurements (binned) of an primary observable A. Let the measured values be $A_1, A_2, ..., A_N$ with the sample average $\overline{A}$. One can obtain the jackknife average of the observable by omitting a single measurement from the sample in all possible ways:

$$A_{(J)s} = \frac{1}{N-1} \sum_{r \neq s} A_r \tag{4.41}$$

The variance of the jackknife estimator of the primary observable is defined as,

$$\sigma^2_{(J)\overline{A}} = \frac{N-1}{N} \sum_{s=1}^{N} (A_{(J)s} - \overline{A}_{(J)})^2 \tag{4.42}$$

where $\overline{A}_{(J)} = \frac{1}{N} \sum_{s=1}^{N} A_{(J)s}$.

Let y be secondary quantity, which is a function of primary quantity A. Corresponding jackknife estimator for the secondary quantity is $y_{(J)s} = y(A_{(J)s})$ with an average

$$\overline{y}_{(J)} = \frac{1}{N} \sum_{s=1}^{N} y_{(J)s}. \tag{4.43}$$

The variance of the jackknife estimator for the secondary quantity is defined as

$$\sigma^2_{(J)\overline{y}} = \frac{N-1}{N}\sum_{s=1}^{N}(y_{(J)s} - \overline{y}_{(J)})^2. \tag{4.44}$$

The jackknife analysis for the secondary quantity gives error estimates $\overline{\overline{y}} = \overline{y} \pm \sigma_{(J)\overline{y}}$.

Bibliography

[1] N. Metropolis *et al.*, *J. Chem. Phys.* **21** 1087 (1953) 78.

[2] A. D. Kennedy and B. J. Pendleton, *Phys. Lett.* **B 156** 393 (1985) 87.

[3] K. Fabricius and O. Haan, *Phys. Lett.* **B 143** 459 (1984) 87.

[4] S. L. Adler, *Phys. Rev.* , **D 38** (1988) 1349.

[5] I. Montvay, G. Münster, *"Quantum Fields on a Lattice"*, Cambridge University Press, Cambridge 1994.

Chapter 5

Noise Reduction Algorithm

In chapter 3 we have seen that the Euclidean expectation values of Wilson loops and their products are the most natural quantities to consider for calculation of the glueball spectrum in non-abelian gauge theory. Numerical computation of loop expectation values and it's correlators in lattice gauge theory is in principle straightforward. The main difficulty in computing large Wilson loops and their correlators is the exponentially decreasing signal-to-noise ratio. Fig. 5.1 shows the temporal separation dependence of the Signal-to-Noise ratio for scalar glueball correlator using bare plaquette.

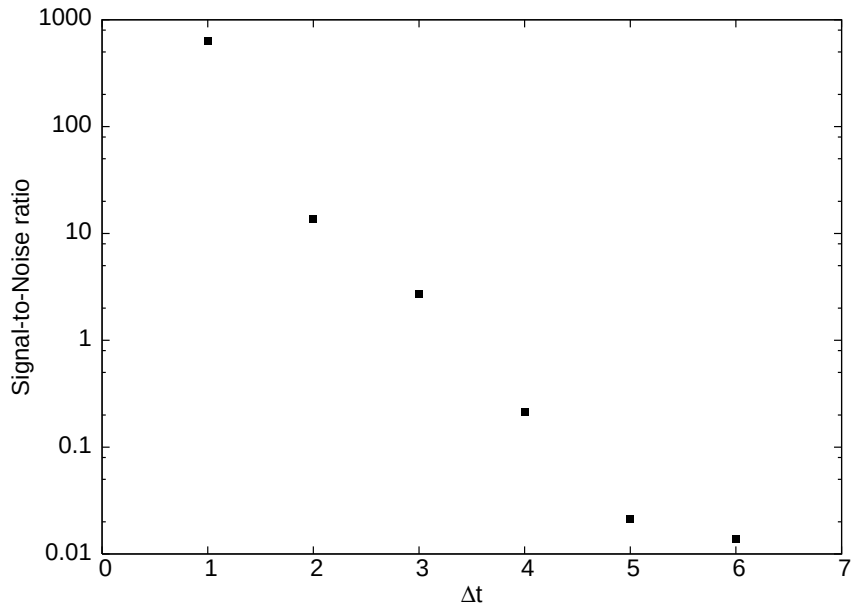

Figure 5.1: Signal-to-Noise ratio for scalar channel glueball using bare plaquette.

Using plaquettes for measuring glueball masses suffers from two problems. First, the overlap of plaquettes with the glueball wave function is poor and this makes the

signal for the correlators weak. Second, they couple strongly to ultraviolet fluctuations, increasing the noise in the correlators. When approaching towards the continuum limit, these problems get worse as the lattice spacing decreases. In [5] it was observed that Wilson loops of size of about 0.5 fm had the strongest overlap with the glueball wave function. Also a large loop is less sensitive to ultraviolet fluctuations.

Better algorithms and computational strategies are needed to handle such problems. A significant improvement is achieved using link blocking techniques and variational methods. In order to get better estimate for ground state glueball masses we need operators which maximise the overlap with the ground state. Operators having extended structure can give better approximation for glueball wave functions even at small lattice spacings. Smearing and Blocking techniques are well developed methods to construct operators with an extended structure. In addition to these methods variational techniques can be used to construct glueball operators with better ground state overlap.

Multilevel algorithms provide a different approach to reduce the statistical noise in glueball correlators. Such algorithms have been used in the past for computing the glueball spectrum for $U(1)$, $SU(2)$ and $SU(3)$ lattice gauge theories. In this chapter we outline this approach. We restrict ourselves to pure Yang-Mills theory with gauge group $SU(3)$ and employ only the standard operators in each J^{PC} channel (scalar and tensor) but try to follow the correlator to large temporal separations using a new noise reduction algorithm. Since the contamination due to excited states falls off exponentially, we expect correlators at distances beyond 0.5 fermi to be dominated by the ground state. Our strategy is to measure glueball correlators at distances beyond 0.5 fm using operators of physical size about 0.5 fm and use the Multilevel algorithm to get signals at large temporal separations.

5.1 Variational Technique

In variational techniques a whole set of operators with different shapes and sizes are used. Let N_0 be the number of such operators $\phi_\alpha^{(R)}(t)$, which transform under same representation R. Using linear combination of these basic operators $\Phi^{(R)}(t)$ can be formed,

$$\Phi^{(R)}(t) = \sum_{\alpha=1}^{N} v_\alpha^{(R)} \phi_\alpha^{(R)}(t) \tag{5.1}$$

The coefficients $v_\alpha^{(R)}$ can be determined by a variational technique [1,2] by minimis-

ing effective mass

$$\tilde{m}(t) = -\frac{1}{t} \ln \frac{\sum_{\alpha\beta} v_\alpha^{(R)} v_\beta^{(R)} \tilde{C}_{\alpha\beta}(t)}{\sum_{\alpha\beta} v_\alpha^{(R)} v_\beta^{(R)} \tilde{C}_{\alpha\beta}(0)} \tag{5.2}$$

where $\tilde{C}_{\alpha\beta}(t)$ is the connected correlator

$$\tilde{C}_{\alpha\beta}(t) = \sum_\tau \langle 0|\tilde{\phi}_\alpha^{(R)}(\tau)\tilde{\phi}_\beta^{(R)}(t+\tau)|0\rangle \tag{5.3}$$

and $\tilde{\phi}_\alpha^{(R)}(\tau) = \phi_\alpha^{(R)}(t) - \langle 0|\phi_\alpha^{(R)}(t)|0\rangle$.

5.2 Anisotropic Lattices

As it is difficult to follow the correlator signal to large physical distances, even using the above techniques, one often uses anisotropic lattices [5] which have a significantly smaller temporal spacing compared to the spatial lattice spacing with the expectation to observe a flat behaviour of the effective mass over several time slices. Improved lattice gauge actions are used to suppress the lattice artifacts from spatially coarse lattices [7] These techniques has been verified to be efficient in calculation of the glueball spectrum [7], and are often adopted. The Glueball mass spectrum using this technique is shown in fig. 5.2

5.3 Multilevel Algorithm

The noise reduction scheme we implement follows the philosophy of the multilevel algorithm [6]. It is a noise reduction method which exploits the local nature of the Wilson gauge action and the existence of a positive definite transfer matrix. This method was used for exponential noise reduction for measuring Polyakov loop correlators and an impressive improvement with respect to the ordinary 1-level algorithm was achieved. However the principle is general and can be applied to other observables as well. In addition to Polyakov loop correlators, it has been used to measure observables such as the Polyakov loop [13], Wilson loop [14], components of the energy-momentum tensor [15] as well as the glueball mass spectrum [4, 5, 7, 9, 11].

The locality property of the Wilson gauge action allows one to quasi-factorise the functional integral for the expectation values and correlators of local observables. In

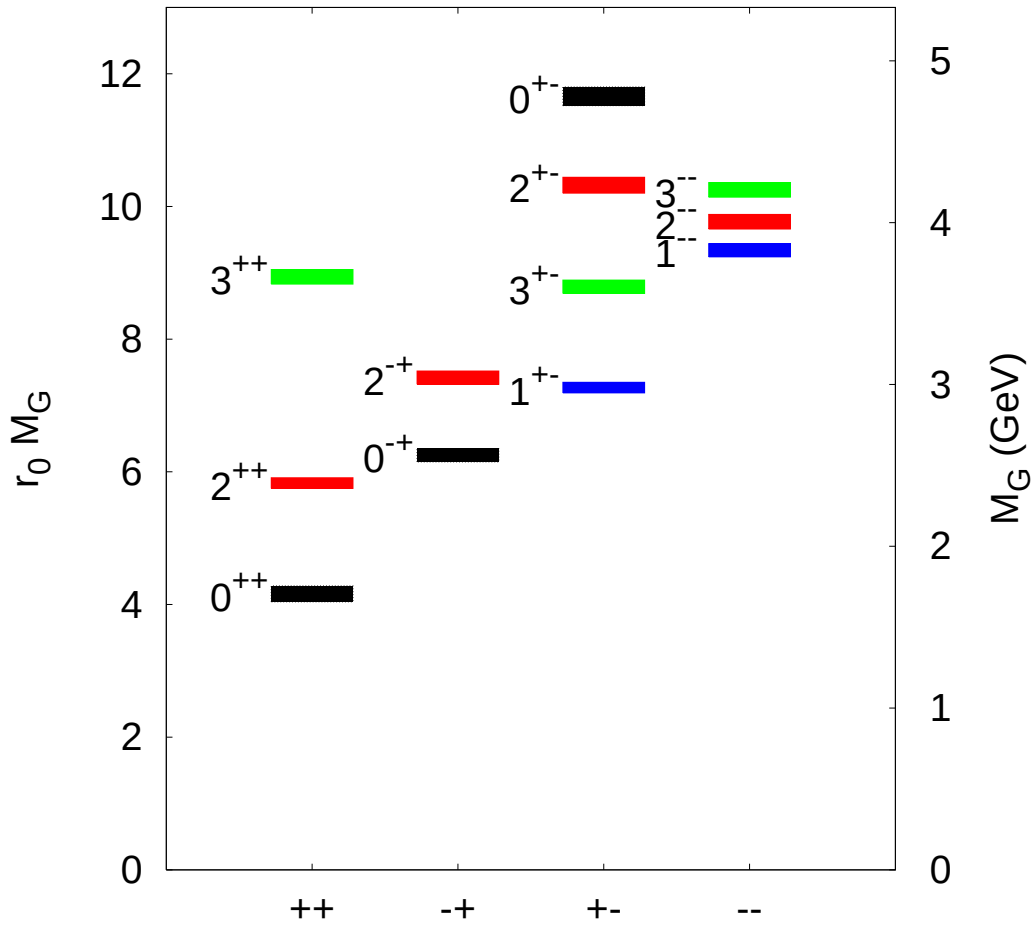

Figure 5.2: The mass spectrum of glueballs in the pure $SU(3)$ gauge theory [7]. The masses are given both in terms of r_0 ($r_0^{-1} = 410$ MeV) and in GeV. The height of each colored box indicates the statistical uncertainty of the mass.

this technique averaging out UV fluctuations separately for each factor makes it efficient. The main principle of the multilevel algorithm is to compute expectation values in a nested manner. Intermediate values are first constructed by averaging over sublattices with boundaries and then the full expectation values are obtained by averaging over the intermediate values with different boundaries. This technique is discussed in some detail in section 5.3.2.

5.3.1 Multihit technique

Our first noise reduction step is a semi-analytic multihit on the $SU(3)$ links [16] with which the Wilson loops are constructed. The multihit technique is a variance reduction technique in which a link is replaced by its expectation value (integral over the group) in a constant background. We elaborate a little on this as this provides a very significant error reduction for us.

In a numerical simulation one can minimize the statistical noise by improved choice of measured quantities. In order to measure the expectation value $\langle O \rangle$, one can choose another quantity O' with the same mean value

$$\langle O' \rangle = \langle O \rangle \tag{5.4}$$

but with smaller variance

$$\sigma^2_{O'} < \sigma^2_O \tag{5.5}$$

where σ^2_O is the variance for the observable O

$$\sigma^2_O = \frac{1}{N-1}[\langle O^2 \rangle - \langle O \rangle^2] \tag{5.6}$$

Let us consider an observable $O[U]$, which depends linearly on the $SU(3)$ link variable U_i and has the form

$$O[U] \equiv \ tr[U_i R[\hat{U}_i]] \tag{5.7}$$

where $\hat{U}_i$ implies all other links except U_i. One can write the Wilson action with the term depending on the link variable U_i as

$$S[U] \equiv -\left(\frac{2}{g^2}\right) \ Re \ tr[U_i A_i] + \hat{S}(\hat{U}_i) \tag{5.8}$$

A_i being the sum of staples for the link variable U_i. The expectation value of the observable O can now be written as

$$\langle O \rangle = \frac{\int [d\hat{U}_i] \ \exp(-\hat{S}(\hat{U}_i)) \ \int dU_i \ \exp[\left(\frac{2}{g^2}\right) \ Re \ tr[U_i A_i]] \ tr[U_i R[\hat{U}_i]]}{\int [d\hat{U}_i] \ \exp(-\hat{S}(\hat{U}_i)) \ \int dU_i \ \exp[\left(\frac{2}{g^2}\right) \ Re \ tr[U_i A_i]]}, \tag{5.9}$$

$$\langle O \rangle = \langle O' \rangle \equiv \frac{\int [d\hat{U}] \exp(-S[\hat{U}]) \ tr\{\overline{U_i} R[\hat{U}_i]\}}{\int [d\hat{U}] \exp(-S[\hat{U}])} \tag{5.10}$$

where $\overline{U_i}$ is the averaged link

$$\overline{U_i} \equiv \ \frac{\int dU_i \ \exp[\left(\frac{2}{g^2}\right) \ Re \ tr \, (U_i A_i)] \ U_i}{\int dU_i \ \exp[\left(\frac{2}{g^2}\right) \ Re \ tr \, (U_i A_i)]} \tag{5.11}$$

Replacing link variable U_i with averaged links $\overline{U_i}$ gives smaller variance. In case of $SU(2)$ the group integration (5.11) can be easily performed using the Bessel function $I_{1,2}$ [18]

$$\overline{U_i} = K_i S_i^{-1} \frac{I_2(\beta K_i)}{I_1(\beta K_i)}. \tag{5.12}$$

For $SU(3)$ gauge theory no analytic method exists for evaluation of group integration (5.11). It must be estimated numerically. A Monte-Carlo with about 10 hits gives acceptable results for $\overline{U_i}$. There exist a semi-analytic method [16] which is about 10 times faster. In this method the one-link integral which depends on the neighbouring links through the source R is defined by

$$Z(R) = \int dU \ \exp[-tr(RU^\dagger + UR^\dagger)], \tag{5.13}$$

where the integration is done over one $SU(3)$ matrix. This one link integral can be expressed as a contour integral of Bessel functions:

$$Z(R) = \oint \frac{dx}{2\pi i} \ e^{xQ} \left(\frac{x}{P(x)}\right)^{\frac{1}{2}} I_1\left(2\left(\frac{P(x)}{x}\right)^{\frac{1}{2}}\right) \tag{5.14}$$

where

$$Q = det \ R + det \ R^\dagger, \tag{5.15}$$

$$P(x) = det(1 + xRR^\dagger). \tag{5.16}$$

The averaged link can be calculated from the one link integral (5.13) as

$$\overline{U} = \frac{\partial}{\partial R} \log Z(R). \tag{5.17}$$

The contour integral (5.14) can be evaluated by performing a gaussian quadrature along a circle centred at the origin with a radius chosen so that one can use the asymptotic expansions of the Bessel functions:

$$I_\nu(Z) = (\frac{e^Z}{\sqrt{2\pi Z}})[1 - \frac{(4\nu^2 - 1)}{8Z} + \frac{(4\nu^2 - 1)(4\nu^2 - 9)}{2!(8z)^2} - \cdots] \tag{5.18}$$

One needs to compromise for the radius which minimizes both the length of the asymptotic expansion and the round-off errors to avoid the conflicting limiting behaviours of the argument $[P(x)/x]^{1/2}$ of the Bessel functions for $|x| \to 0$ and $|x| \to \infty$.

5.3.2 2-level algorithm for glueballs

For our implementation, we slice the lattice along the temporal direction by fixing the spatial links and compute the intermediate expectation values of the glueball operators by performing several sub-lattice updates. Individual correlators are created using products of the averaged operators at different time slices. The scheme is depicted in Fig. 5.3.

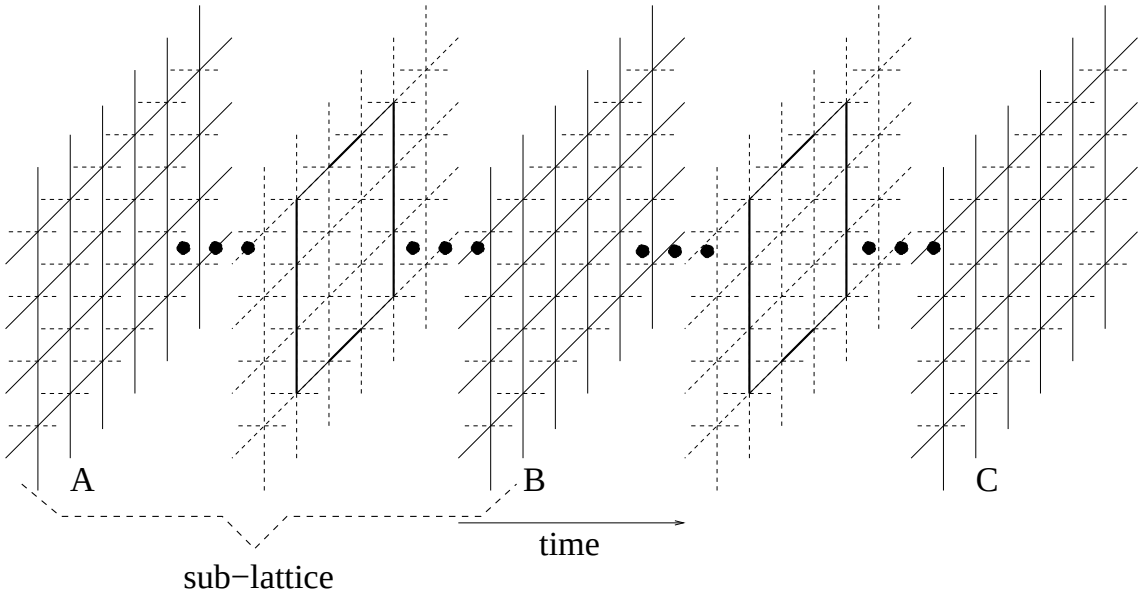

Figure 5.3: Multilevel scheme for computing glueball correlators. The time slices marked A, B and C are held fixed during the sub-lattice updates. The thick links are the ones which are replaced by their multihit averages.

The glueball operators between which we compute our correlation function (source and sink) are extended Wilson loops denoted by P_{ab} where a, b go over the three spatial directions x, y, z. The operators are projected to zero momentum states. We denote the temporal separation between the source and the sink operator by Δt. Our lattices are of size $N_x \times N_y \times N_z \times N_t$. For each set of sub-lattice updates, $\frac{N_t}{\Delta t}$ time slices separated by distance Δt are kept fixed. Average values of the operators $\langle \mathcal{P}(t) \rangle_{bc}$ are calculated for all time-slices between the fixed time-slices. After each set of sub-lattice updates, n_{sp} number of sweeps over the entire lattice was performed to remove auto-correlation between consecutive compound measurements. After n_{meas} number of these compound measurements the correlators are computed as

$$\langle \mathcal{P}(t_i)\mathcal{P}(t_j) \rangle = \frac{1}{n_{meas}} \sum_{bc} \langle \mathcal{P}(t_i) \rangle_{bc} \langle \mathcal{P}(t_j) \rangle_{bc} \tag{5.19}$$

Correlation functions between large loops have the advantage that they have much less contamination from the higher excited states compared to those between elementary plaquettes. Such an approach was reported in [5]. There, however, single exponential fits to the correlators were not possible as the data was too noisy. Nevertheless it was observed that glueballs seemed to have the largest overlap with loops of spatial extent 0.5 fermi in each direction. We therefore choose [17] loops of roughly of the same extent to construct our glueball operators.

The parameters for our simulations are the lattice size, the lattice scale r_0/a, size of the Wilson loops and the number of sub-lattice updates. These parameters along with the number of compound measurements are given in Table 5.1.

Lattice	Size	β	(r_0/a)	sub−lattice thickness	iupd	loop size	# meas.
A	$10^3 \times 18$	5.70	2.922(9)	3	30	2×2	1000000
B	$12^3 \times 18$	5.80	3.673(5)	3	25	3×3	1248000
C	$16^3 \times 20$	5.95	4.898(12)	4	50	5×5	1024000
D‡	$18^3 \times 30$	6.07	6.033(17)	6	60	5×5	225000
E‡	$24^3 \times 32$	6.20	7.380(26)	8	65	8×8	309000
F‡	$30^3 \times 40$	6.40	9.74(5)	10	70	10×10	256300
D	$12^3 \times 18$	5.80	3.673(5)	3	70	3×3	5760000
E	$12^3 \times 20$	5.95	4.898(12)	5	100	5×5	3456000
F	$12^3 \times 20$	6.07	6.033(17)	5	100	5×5	1536000
G	$18^3 \times 30$	6.07	6.033(17)	6	500	6×6	425120
H	$24^3 \times 32$	6.20	7.380(26)	8	400	8×8	184000
I	$30^3 \times 40$	6.40	9.74(5)	10	400	10×10	121600

Table 5.1: Simulation parameters for all the lattices. Lattices A, B, C, D‡, E‡ and F‡ were used for the scalar channel while D, E, F, G, H and I were for the tensor channel.

The choice of the number of sub-lattice updates "iupd" is an important parameter of this algorithm. For the tensor channel, the rule of the thumb we follow is that the operator expectation value over the sub-lattice updates should be the same order as the square root of the correlator at a large value of Δt. For the scalar channel the same holds but for the connected parts.

The multilevel algorithm is very efficient for calculating quantities with very small expectation values. While the operators in the tensor channel viz. $\mathcal{E}_1 = Re(\mathcal{P}_{xz} - \mathcal{P}_{yz})$ and $\mathcal{E}_2 = Re(\mathcal{P}_{xz} + \mathcal{P}_{yz} - 2\mathcal{P}_{xy})$ have zero expectation values and are therefore ideal

for direct evaluation using the multilevel scheme, the scalar operator $\mathcal{A} = Re(\mathcal{P}_{xy} + \mathcal{P}_{xz} + \mathcal{P}_{yz})$ has a non-zero expectation value which has to be subtracted to obtain the connected correlator. For the scalar channel, we therefore do the simulation in two steps. The first step is to determine the expectation value of the glueball operator. This has to be determined very accurately so that the error in the expectation value has negligible contribution to the error on the correlator. Otherwise the error on the expectation value of the operator will dominate the total error and further error reduction on the correlator would be impossible. We use multi-hit on the links to determine the expectation value of the glueball operator. While this was sufficient for our loop size and coupling, if necessary a multi-level scheme can also be used for this estimate. Then we directly computed the connected correlator using $(\mathcal{A} - \langle\mathcal{A}\rangle)$ as the operator with a zero expectation value. Where the expectation value $\langle\mathcal{A}\rangle$ is determined by taking average over the operator expectation values on all the time-slices.

$$\langle\mathcal{A}\rangle = \frac{1}{N_t}\sum_{t=1}^{N_t}\langle\mathcal{A}(t)\rangle \tag{5.20}$$

The choice of "iupd" was done in the same way as in the tensor channel.

For the scalar channel there exists an alternative method [9] to avoid that two step process by taking the derivative of the correlator. Taking derivative of the correlator $C_{conn}(t, t_0)$ at both t and t_0 one obtains,

$$\partial_t\partial^*_{t_0}\ (C_{conn}(t,t_0)) \approx -\alpha[e^{-m(t-t_0)}(1-e^{-m})^2\ +\ e^{-m(N_t-(t-t_0))}(e^m-1)^2] \tag{5.21}$$

where ∂_t be the forward derivative and ∂_{t_0} be the backward derivative. On the lattice we measure,

$$\begin{aligned}\partial_t\partial^*_{t_0}\,(C_{conn}(t,t_0)) = \langle Re\sum_{n,i<j}[P_{ij}(n,t+1) - P_{ij}(n,t)]\times \\ Re\sum_{n,i<j}[P_{ij}(n,t_0) - P_{ij}(n,t_0-1)]\rangle\end{aligned} \tag{5.22}$$

where $P_{ij}(n,t)$ denotes the plaquette in ij plane at lattice site n on time-slice t and $[\cdots]$ denotes sublattice average of a quantity. The derivatives are estimated in the sublattice updates by taking the difference of the value of the operator on the updated slice with the value of the operator on the boundary. As shown in Fig. 5.4, to get the forward derivative at t, we used the fixed boundary at $(t+1)$ and for the backward derivative, the boundary at $(t-1)$. To get the correlators one has to use two such slices (e.g., t and t_0 in Fig. 5.4). In practice we hold every alternate layer of spatial links fixed and estimate the correlators for various time separations at the same time.

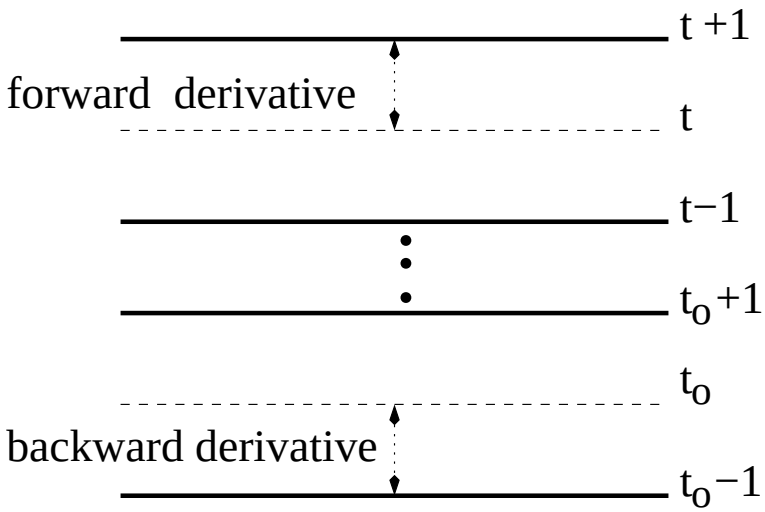

Figure 5.4: Evaluation of the derivative of the glueball correlator. The thick lines are held fixed during the sub-lattice averaging.

We observed one more phenomenon which is particular to this algorithm. For the smaller values of t where most contributions come from slices which are within the same sub-lattice, there are strong effects due to the short temporal extent of the sub-lattice itself. In such cases we were forced to take into account only correlators between those time slices which lay in different sub-lattices. We found this effect to be significant only in the tensor channel (probably because of the larger value of iupd in those cases).

Bibliography

[1] C. J. Morningstar and M. J. Peardon, *Phys.Rev.* **D56** (1997) 4043-4061.

[2] M. Lüscher and U. Wolff, *Nucl. Phys.***B339** (1990) 222.

[3] C. J. Morningstar and M. J. Peardon, *Phys. Rev.* **D60** (1999) 034509 [arXiv:hep-lat/9901004].

[4] Y. Chen *et. al.*, *Phys. Rev.* **D73** (2006) 014516 [arXiv:hep-lat/0510074].

[5] R. Gupta *et al.*, *Phys. Rev.* **D43** (1991) 2301.

[6] M. Lüscher and P. Weisz, *JHEP*, **0109** (2001) 010 [arXiv:hep-lat/0108014].

[7] H. B. Meyer, *JHEP* **0301** (2003) 048 [arXiv:hep-lat/0209145]

[8] H. B. Meyer, *JHEP* 0401 (2004) 030 [arXiv:hep-lat/0312034].

[9] P. Majumdar, Y. Koma, M. Koma, *Nucl. Phys.* **B677** (2004) 273 [arXiv:hep-lat/0309006].

[10] H. B. Meyer, *JHEP* **0901** (2009) 071 [arXiv:hep-lat/0808.3151].

[11] H. B. Meyer, M. J. Teper, *Phys. Lett.* **B605** (2005) 344 [arXiv:hep-ph/0409183].

[12] M. Della Morte, L. Giusti, *JHEP* **1105** (2011) 056 [arXiv:hep-lat/1012.2562].

[13] D. Banerjee *et. al.*, *Phys. Rev.* **D85** (2012) 014510 [arXiv:hep-lat/1109.5738].

[14] P. Majumdar, *Nucl. Phys.* **B664** (2003) 213 [arXiv:hep-lat/0211038].

[15] H. B. Meyer, *Phys. Rev.* **D76** (2007) 101701 [arXiv:hep-lat/0704.1801].

[16] Ph. de Forcrand and C. Roiesnel, *Phys. Lett.* **B151** (1985) 77.

[17] P. Majumdar, N. Mathur, S. Mondal, *Phys. Lett.* **B736** (2014) 415 [arXiv:hep-lat/1403.2936].

[18] I. Montvay, G. Münster, *"Quantum Fields on a Lattice"*, Cambridge University Press, Cambridge 1994.

Chapter 6

Results

In this chapter we describe the results for glueball masses obtained using the 2-level algorithm. We also discuss methods to extract glueball masses from the measured correlators and the efficiency of our algorithm.

6.1 Algorithmic Gain

Lattice	Size	β	th	iupd	loop size
A_1	$6^3 \times 16$	5.7	2	20	2×2
B_1	$6^3 \times 18$	5.8	3	25	3×3
C_1	$8^3 \times 24$	5.95	4	50	5×5
D_1	$6^3 \times 18$	5.8	3	50	3×3
E_1	$8^3 \times 30$	5.95	5	100	5×5
F_1	$10^3 \times 30$	6.07	6	130	6×6

Table 6.1: Simulation parameters for additional lattices on which comparisons with the naive method were carried out. Lattices A_1,B_1 and C_1 were used for the scalar channel while D_1,E_1 and F_1 were for the tensor channel. (th denotes the sub-lattice thickness)

To investigate the advantage of the current algorithm over the naive method, we did a few runs for the same computer time using both methods. Since it is not clear a-priori how the algorithm behaves as either Δt or β changes we report our experience for different values of Δt and β (see Table 6.2). The lattice parameters we used for this test are summarized in table 6.1.

For the lattice D1 , we carried out runs for 200 hours. The multilevel algorithm had an error of 3% at $\Delta t = 3$ which is just below r_0 (see Table 6.2), while the naive algorithm had an error of 81%. It would be interesting to compare the performance at a value of Δt between r_0 and $2r_0$. So we choose points around $1.5r_0$ (in this case $\Delta t = 6$). Even after 200 hours of runtime we did not have a signal at that distance for the naive method. So to estimate the % error we multiply the naive correlator at the largest value of Δt where we have a signal (i.e. $\Delta t = 3$) by $\frac{corr_{multilevel}(\Delta t=6)}{corr_{multilevel}(\Delta t=3)}$. Doing this, we get the % error to be 850% for the naive method while it is 29% for the multilevel scheme. Thus for the tensor channel at $\beta = 5.8$ we estimate that the error reduction algorithm produces an error which is between 27 times smaller than the naive method at both t = 3 and 6. Since the $error \propto time^2$ we estimate the new method is more efficient by at least a factor of 729 or so.

Scalar channel				Tensor channel			
#	time (min)	$\frac{\text{err}_\text{n}}{\text{err}_\text{ml}}$	*gain*	#	time (min)	$\frac{\text{err}_\text{n}}{\text{err}_\text{ml}}$	*gain*
A	3850	5.7	32	D_1	12000	27	729
B_1	1000	5.5	30	E_1	5775	20	400
C_1	1100	18	324	F_1	15000	–	–

Table 6.2: Comparison of error bars between the naive and error reduction methods. err_n stands for error in the naive method while err_ml denotes error in the multilevel scheme. *gain* is in terms of time and is given by $(\text{err}_\text{n}/\text{err}_\text{ml})^2$.

At $\beta = 5.95$ (lattice E1), the runs were for about 100 hours. There at $\Delta t = 3$ the multilevel algorithm produced an error of about 4% while the naive algorithm had an error of 75%. Doing a similar estimate as $\beta = 5.8$ we estimate that at $1.5r_0$ ($\Delta t = 8$) the errors are 150% for the multilevel algorithm while it is about 3000% for the naive method. At this β value therefore, the gains in terms of % error is about a factor 20. At $\beta = 6.07$, we did not get a signal for the naive algorithm for any t other than $\Delta t = 1$ even after about 300 hours of runs. Thus we see that the gain has very little dependence on t but does depend on β.

For the scalar channel using lattice A, runs were carried out for about 3850 min. Comparing the errors around $1.4r_0$, we got a gain of about 5.7 in terms of errors or 32 in terms of time. At $\beta = 5.8$ (lattice B1) the runs were carried out for about 1000 min.

In this case we have a signal at $1.5r_0$ for both methods and we get an error of 13% for the multilevel scheme while it is about 70% for the naive method. Thus the gain in terms of % error is about 5.5 or in terms of time about 30. At $\beta = 5.95$ in the scalar channel, again we do not have a signal at $1.5r_0$ using the naive method and are forced to use the same method as in the tensor channel to estimate the errors. At $\Delta t = 3$ we obtain the errors to be 2% and 37% for the multilevel and the naive methods respectively while at $1.5r_0$ they are 29% and 500% (estimated) respectively. Thus the ratio of errors is about 18 or gain in terms of time 324.

In addition to the above, at $\beta = 5.7$ we have one more comparison using the lattice A_1. There we obtain a gain of 2.5 in terms of errors or 6 in terms of time. Thus the gain seems to increase with increase in volume. We expect this will help us go to larger lattices.

6.2 Fitting Strategy and Masses

For most of our lattices we extracted the glueball masses using the standard correlators and fitting them to the form

$$C(\Delta t) = A[\exp(-m\Delta t) + \exp(-m(T - \Delta t))] \tag{6.1}$$

where m is the glueball mass and T is the full temporal extent of the lattice. Since the correlator is symmetric about $T/2$ we folded the data about $T/2$ and used only one half of the temporal range for the fits.

In this section we describe our fitting procedures and the masses we obtain. In addition, for $\beta = 5.7$ we computed the derivative of the correlator using eqn. (5.22). We extracted the mass by fitting the derivative of the correlator to the form (5.21). From this fitting we obtained the scalar glueball mass $m_{0^{++}}a = 0.924(033)$ with $\chi^2/d.o.f = 1.18$. We did not include this mass for the scalar channel, as this calculation was done for a smaller lattice volume.

For fitting we used the "non-linear model fit" of Mathematica and the fit range was decided on the following two criteria: (i) the range should extend to as large a value of Δt as possible and (ii) the fit to the form in Eq. (1) should have a p-value < 0.01 for both m and A. We found that the p-value for A gave the most stringent criterion for accepting the fit. The fit range for all the different channels and couplings along with

the $\chi^2/d.o.f.$ are indicated in Tables 6.3, 6.4 , 6.5 and 6.6.

We took $\langle C(\Delta t)\rangle$ in eq. (6.1) to be a jackknife average over 20 bins and checked that this data set was independent of autocorrelation. However there is another correlation in the fitting procedure *viz.* that the different values of Δt are correlated as they are drawn from a single sample. The correlation between different temporal separations is characterized by the covariance matrix

$$Cov_N(\Delta t, \Delta t') = \frac{1}{N}\langle (C(\Delta t) - \langle C(\Delta t)\rangle_N)(C(\Delta t') - \langle C(\Delta t')\rangle_N)\rangle_N \tag{6.2}$$

where N is the number of bins. The central limit theorem suggests that the distribution of independent random variables are Gaussian. The best fit is defined as maximum likelihood corresponding to minimum of χ^2 defined as

$$\chi^2 = \sum_{\Delta t, \Delta t' = \Delta t_{min}}^{\Delta t^{max}} (C(\Delta t) - \langle C(\Delta t)\rangle_N)\omega(\Delta t, \Delta t')(C(\Delta t') - \langle C(\Delta t')\rangle_N), \tag{6.3}$$

where $\omega(\Delta t, \Delta t') = Cov_N^{-1}(\Delta t, \Delta t')$. If the bins are jackknife samples the covariance matrix is

$$Cov_{(J)n}(\Delta t, \Delta t') = \frac{n-1}{n}\langle (\overline{C}(\Delta t) - \overline{\overline{C}}(\Delta t))(\overline{C}(\Delta t') - \overline{\overline{C}}(\Delta t'))\rangle_n \tag{6.4}$$

where $\overline{C}(\Delta t)$ is the jackknife bin average of the correlator for each bin, $\overline{\overline{C}}(\Delta t)$ is the jackknife average over n bins. The "non-linear model fit" of Mathematica cannot handle correlated fits directly. Therefore for our correlated fits we minimized the corelated χ^2 for each jackknife bin using NMinimize of Mathematica. This gave us a set of values for the mass and we computed the mean value and jackknife error from this set. While our primary results are from uncorrelated fits, we performed correlated fits wherever possible to check that the uncorrelated fits do not grossly underestimate the error on the fit parameters. In most cases we found the error on the fit parameters to be comparable for the correlated and uncorrelated fits. Our correlated fits are reported in tables 6.4 and 6.6. Sometimes statistical fluctuations can generate small eigenvalues of $Cov_N(\Delta t, \Delta t')$. These can destabilize the fit. In such cases we used the diagonal part of the covariance matrix. The latter gives rise to $\omega(\Delta t, \Delta t') = \delta_{\Delta t, \Delta t'}/\sigma(\Delta t)^2$ and the χ^2 functional reduces to the form familiar from uncorrelated fits.

Global fit for the Scalar Channel					
	global fit			effective mass	
#	range	ma	$\frac{\chi^2}{d.o.f}$	t-slice	ma
	2-9	0.981(3)	1.8	2/3	0.991(2)
	3-9	0.961(2)	0.05	3/4	0.977(6)
A	4-9	0.962(5)	0.06	4/5	0.966(22)
	5-9	0.952(11)*	0.066	5/6	0.957(41)
				6/7	0.89(12)
	2-9	0.936(4)	5.7	2/3	0.944(1)
	3-9	0.915(2)	0.3	3/4	0.919(4)
B	4-9	0.904(2)	0.05	4/5	0.899(8)
	5-9	0.911(3)	0.025	5/6	0.909(21)
	6-9	0.906(8)*	0.03	6/7	0.899(53)
	3-10	0.765(3)	1.3	2/3	0.822(1)
C	4-10	0.7537(9)	0.04	3/4	0.773(2)
	5-10	0.7510(15)*	0.02	4/5	0.755(4)
	6-10	0.7499(38)	0.03	5/6	0.751(9)
				6/7	0.734(20)
				7/8	0.723(39)
	4-9	0.640(7)	1.317	2/3	0.692(3)
D‡	5-9	0.618(7)	0.734	3/4	0.667(5)
	6-10	0.596(5)*	0.11	4/5	0.655(7)
	6-9	0.598(5)	0.104	5/6	0.634(12)
	5-10	0.617(7)	0.702	6/7	0.606(26)
				7/8	0.569(73)
	6-11	0.538(13)	1.734	2/3	0.618(3)
	6-12	0.537(11)∗	1.424	3/4	0.575(5)
E‡	7-11	0.502(10)	0.332	4/5	0.554(7)
	7-12	0.503(8)	0.256	5/6	0.528(9)
				6/7	0.579(23)
				7/8	0.503(26)
	7-15	0.4157(47)	0.42	2/3	0.560(4)
	8-16	0.4091(77)∗	0.49	3/4	0.467(6)
F‡	8-15	0.4108(74)	0.44	4/5	0.444(8)
	9-15	0.414(12)	0.67	5/6	0.418(8)
	9-16	0.411(13)	0.56	6/7	0.418(15)
Continued on next page					

Continued from previous page

	global fit			effective mass	
#	range	ma	$\frac{\chi^2}{d.o.f}$	t-slice	ma
	10-16	0.416(21)	0.49	7/8	0.427(18)
				8/9	0.408(33)

Table 6.3: Glueball masses for the scalar channel in lattice units (a denotes the lattice spacing) for all lattices along with the fit parameters. A * on the mass denotes our best estimate for a particular coupling and channel.

Correlated fit for the Scalar Channel					
	correlated fit			effective mass	
#	range	ma	$\frac{\chi^2}{d.o.f}$	t-slice	ma
	3-9	0.9172(1)	1.15-1.87	2/3	0.944(1)
	4-9	0.8969(4)	0.08-0.52	3/4	0.919(4)
B	5-9	0.9115(10)	0.016-0.19	4/5	0.899(8)
	6-9	0.9193(22)	0.04-0.27	5/6	0.909(21)
	7-9	0.8851(48)	0.01-0.19	6/7	0.899(53)
	4-10	0.75584(14)	0.07-0.49	2/3	0.822(1)
	5-10	0.75172(42)	0.06-0.45	3/4	0.773(2)
C	6-10	0.74579(70)	0.03-0.34	4/5	0.755(4)
	7-10	0.74854(90)	0.06-0.46	5/6	0.751(9)
				6/7	0.734(20)
				7/8	0.723(39)
	4-10	0.6598(3)	0.85-1.56	2/3	0.692(3)
D‡	5-10	0.6426(6)	0.38-0.97	3/4	0.667(5)
	6-10	0.6052(12)	0.05-0.3	4/5	0.655(7)
	7-10	0.5907(20)	0.015-0.176	5/6	0.634(12)
				6/7	0.606(26)
				7/8	0.569(73)
	6-12	0.5555(7)	1.18-1.89	2/3	0.618(3)
	7-12	0.5121(11)	0.39-0.937	3/4	0.575(5)
E‡	8-12	0.5005(21)	0.48-1.14	4/5	0.554(7)

Continued on next page

Continued from previous page					
	correlated fit			effective mass	
#	range	ma	$\frac{\chi^2}{d.o.f}$	t-slice	ma
	9-12	0.4697(27)	0.31-1.23	5/6	0.528(9)
	10-12	0.4312(38)	0.35-1.41	6/7	0.579(23)
				7/8	0.503(26)
	7-16	0.4280(6)	0.71-1.87	2/3	0.560(4)
	8-16	0.4045(99)	0.65-1.29	3/4	0.467(6)
F‡	9-16	0.4087(18)	0.71-1.12	4/5	0.444(8)
	10-15	0.4165(26)	0.82-1.69	5/6	0.418(8)
	10-16	0.4112(27)	0.83-1.63	6/7	0.418(15)
				7/8	0.427(18)
				8/9	0.408(33)

Table 6.4: Glueball masses for the scalar channel in lattice units (a denotes the lattice spacing) for all lattices along with the fit parameters.

Global fit for the Tensor Channel					
	global fit			effective mass	
#	range	ma	$\frac{\chi^2}{d.o.f}$	t-slice	ma
	2-7	1.758(9)	32.2	2/3	1.763(2)
D	3-7	1.656(12)	1.98	3/4	1.661(14)
	4-7	1.585(54)∗	1.64	4/5	1.605(49)
				5/6	1.39(19)
	4-10	1.166(13)	3	2/3	1.311(1)
E	5-10	1.115(39)	2.4	3/4	1.223(3)
	6-10	0.938(17)∗	0.12	4/5	1.177(8)
				5/6	1.152(20)
				6/7	0.951(52)
	4-10	0.988(10)	3.3	2/3	1.177(1)
F	5-10	0.929(10)	0.44	3/4	1.070(2)
	6-10	0.885(16)∗	0.16	4/5	1.004(7)
Continued on next page					

Continued from previous page					
	global fit			effective mass	
#	range	ma	$\frac{\chi^2}{d.o.f}$	t-slice	ma
				5/6	0.939(10)
				6/7	0.899(46)
				7/8	0.869(89)
	6-9	0.967(19)∗	1.15	2/3	1.139(1)
	7-9	0.885(8)	0.02	3/4	1.044(2)
G	7-10	0.873(32)	0.38	4/5	1.006(6)
				5/6	0.984(26)
				6/7	1.008(20)
				7/8	0.842(180)
				8/9	0.842(192)
	6-10	0.744(9)∗	0.69	2/3	1.015(2)
	7-10	0.763(17)	0.58	3/4	0.885(3)
	8-10	0.746(57)	1.05	4/5	0.840(5)
H	8-11	0.728(46)	0.83	5/6	0.802(12)
				6/7	0.760(20)
				7/8	0.719(87)
				8/9	0.857(121)
	8-12	0.600(7)	0.19	2/3	0.911(2)
	8-13	0.600(6)	0.14	3/4	0.742(3)
	9-13	0.602(12)	0.19	4/5	0.673(6)
	10-13	0.574(18)∗	0.19	5/6	0.649(9)
I	11-13	0.620(3)	0.0006	6/7	0.638(16)
				7/8	0.625(26)
				8/9	0.643(59)
				9/10	0.722(153)

Table 6.5: Glueball masses for the tensor channel in lattice units (a denotes the lattice spacing) for all lattices along with the fit parameters. A * on the mass denotes our best estimate for a particular coupling and channel.

In addition to masses from global fits, we also compute the effective masses from

the correlators as

$$am_{eff} = -\ln \frac{\langle C(\Delta t + 1)\rangle}{\langle C(\Delta t)\rangle} \tag{6.5}$$

where a is the lattice spacing. To estimate the error on the effective masses we take $\langle C(\Delta t)\rangle$ to be a jackknife bin and we compute masses for 20 such bins. The error on the effective mass is the jackknife error computed from the spread of the masses from the different bins. The effective masses are also reported in Tables 6.3, 6.4, 6.5 and 6.6.

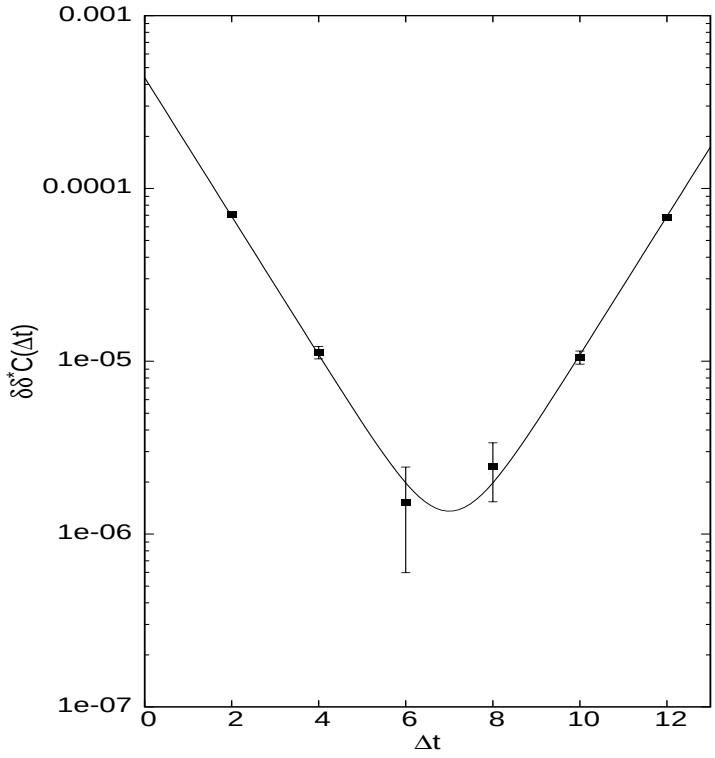

Figure 6.1: Derivative of the scalar glueball correlator $\partial\partial^* C(\Delta t)$ against Δt for $\beta = 5.7$

In Fig. 6.1 we plot the derivative of the scalar correlator for $\beta = 5.7$. In Fig. 6.2 to Fig. 6.13 we plot the standard correlators along with the respective fits for each channel and coupling. Even though the fits were done on the folded data, in the figures we plot the fitted correlator over the full range. It can be clearly seen, especially in the tensor channel that the correlators have contamination from the excited states for the smaller values of Δt. The same thing is seen for the effective masses. The masses fall at first and then stabilize to a plateau albeit with increasing error bars for larger values of Δt.

We cross-check our data by comparing them with results in [1, 3–5, 7]. The comparison is given in Table 6.7 and Table 6.8. In [1] scalar and tensor glueball masses

were computed on a symmetric lattice with the Wilson action in the β range 5.6925 to 6.3380 and we compared mostly with the data presented there using exponential interpolation wherever necessary. To interpolate the data between two values of β we used the formula [1]

$$y = c(\frac{d}{c})^{(\frac{x-a}{b-a})}. \tag{6.6}$$

Here c and d are known values of the data for the β values of a and b respectively. Then at x ($a \leq x \leq b$) the interpolated value of the data is given by y.

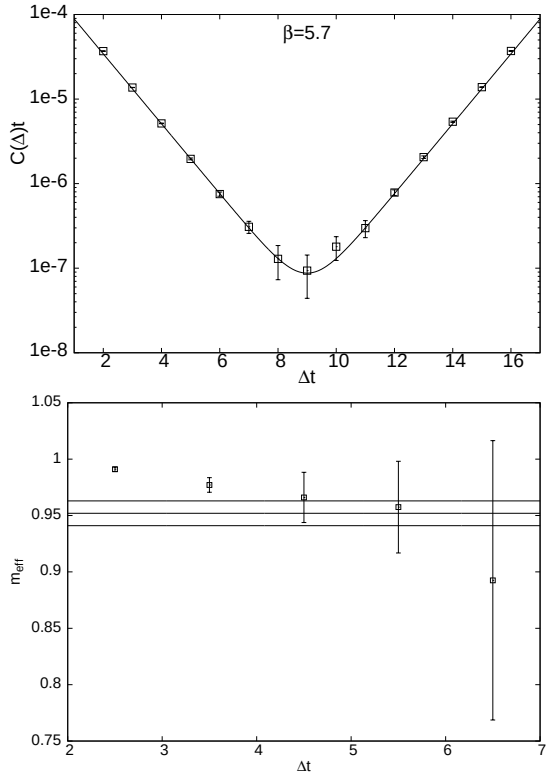

Figure 6.2: The correlator along with it's fit (fit range : 5-9) and the effective mass plot at the $\beta = 5.7$ for the scalar channel.

In the scalar channel at $\beta = 5.6925$ & 5.6993 the masses obtained were 0.941(25) and 0.969(18) respectively. In [4] the same mass at $\beta = 5.7$ was computed to be 0.929(49) and in [7], from the ratio of partition functions, as 0.935(42). These compare quite well with our global fit value of 0.952(11) at $\beta = 5.7$. The effective masses we obtain are also consistent with this value.

[1] Glueball masses in lattice unit scales near continuum limit as $am = C_m \exp\left(-\frac{1}{2\beta_0 g^2}\right)(\beta_0 g^2)^{-\frac{\beta_1}{2\beta_0^2}}(1 + \mathcal{O}(g^2))$ [3], where β_0, β_1 are coefficients of the power series expansion of the β-function, which is different from the lattice inverse coupling $\beta \sim \frac{1}{g^2}$. This scaling behaviour justifies the use of exponential interpolation formula instead of the linear one.

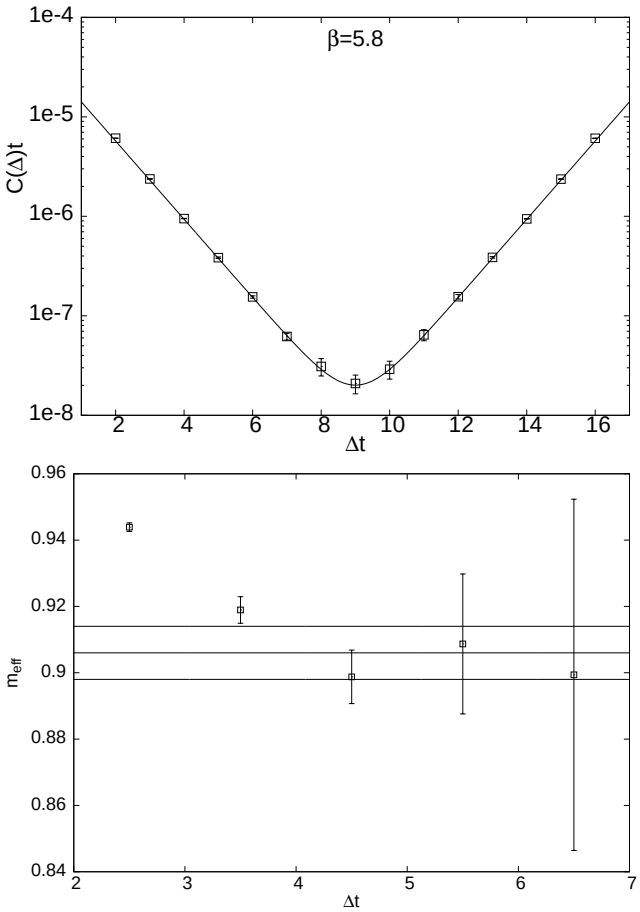

Figure 6.3: The correlator along with it's fit (fit range : 6-9) and the effective mass plot at $\beta = 5.8$ for the scalar channel.

For the scalar channel at $\beta = 5.8$ we compared our data with [1]. At $\beta = 5.7995$ & 5.8, [1] reports values for scalar masses as 0.909(15) and 0.945(21). For $\beta = 5.8$ we obtain from the global fit 0.906(8) which is in good agreement with [1]. Our effective mass plot indicates significant contribution from excited states are present till $\Delta t = 4$.

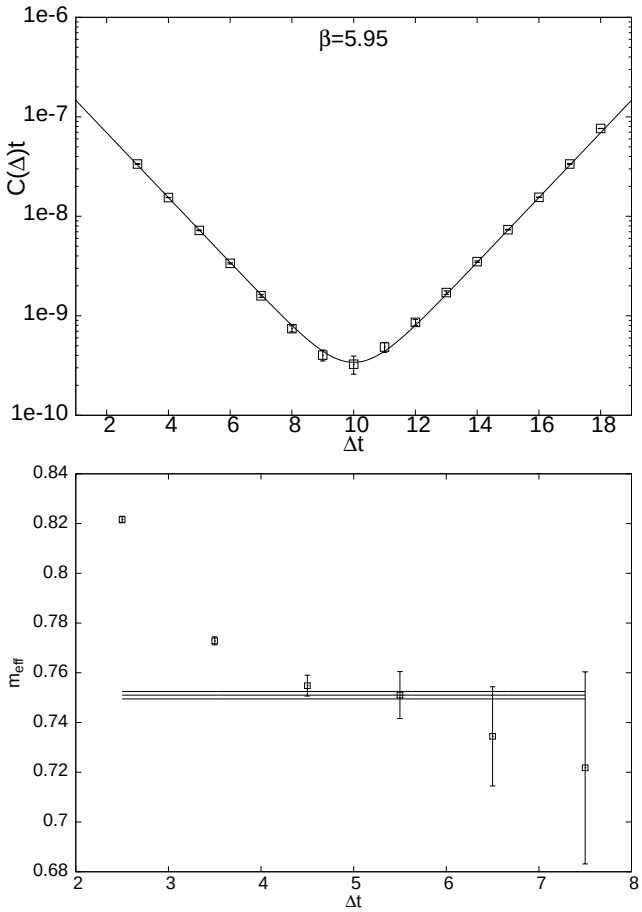

Figure 6.4: The correlator along with it's fit (fit range : 5-10) and the effective mass plot at the $\beta = 5.95$ for the scalar channel.

At $\beta = 5.95$ we obtain, using interpolation, a value of 0.743(12) from the results in [1]. Our global fit to the correlator gives us a value of 0.7510(15) and our effective mass values are also consistent with this estimate. Excited state contamination seems to be present till $\Delta t = 4$.

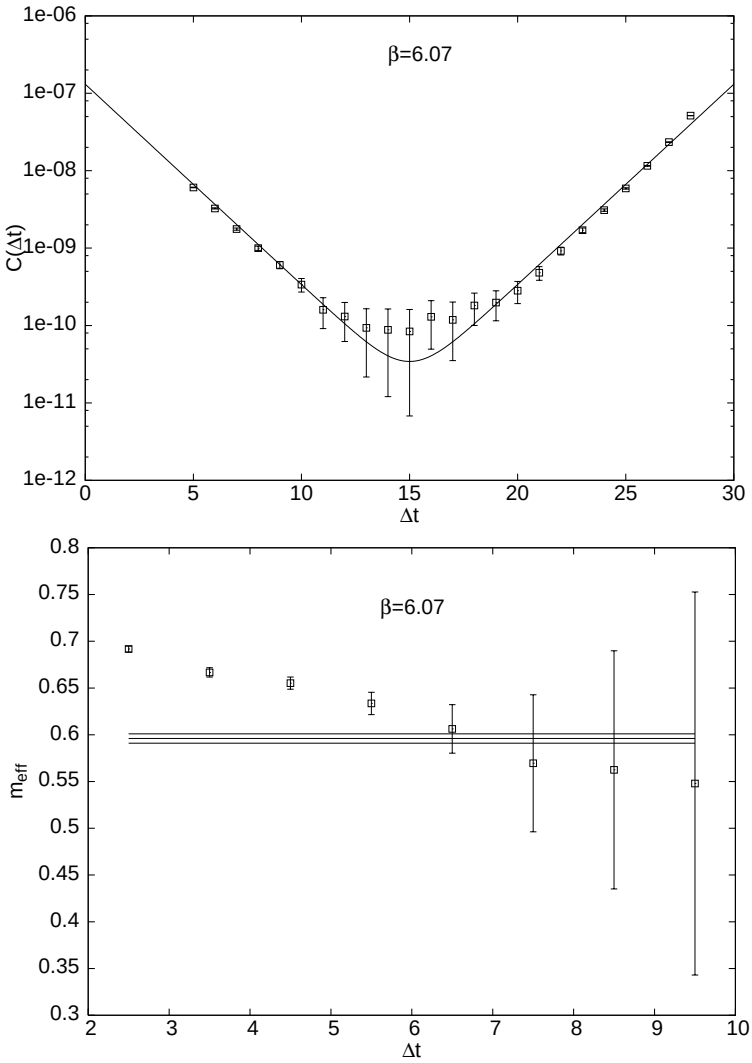

Figure 6.5: The correlator along with it's fit (fit range : 6-10) and the effective mass plot at the $\beta = 6.07$ for the scalar channel.

The scalar glueball mass was computed at $\beta = 6.00$ and $\beta = 6.10$ in [3]. At $\beta = 6.07$ we obtain, using interpolation, a value of 0.6301(77) from the results in [3]. The scalar glueball mass obtained from global fit of our calculation was $ma = 0.596(5)$. Again effective masses indicate significant contribution of excited states till $\Delta t = 5$.

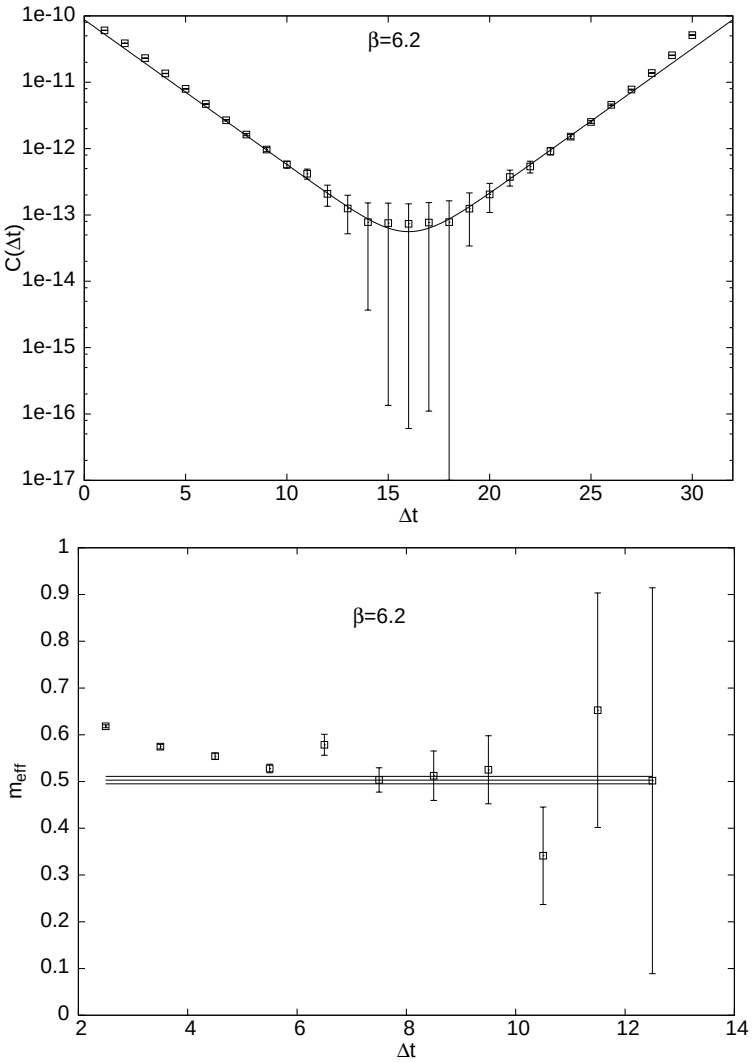

Figure 6.6: The correlator along with it's fit (fit range : 6-12) and the effective mass plot at the $\beta = 6.2$ for the scalar channel.

For $\beta = 6.2$ we compared our data with table 1 of [3]. At $\beta = 6.2$ [3] reports the value of scalar glueball mass $ma = 0.5197(51)$. From the global fit of the correlator we obtain the value of scalar glueball mass $ma = 0.503(8)$. Contamination from excited states seems to persist till $\Delta t = 6$.

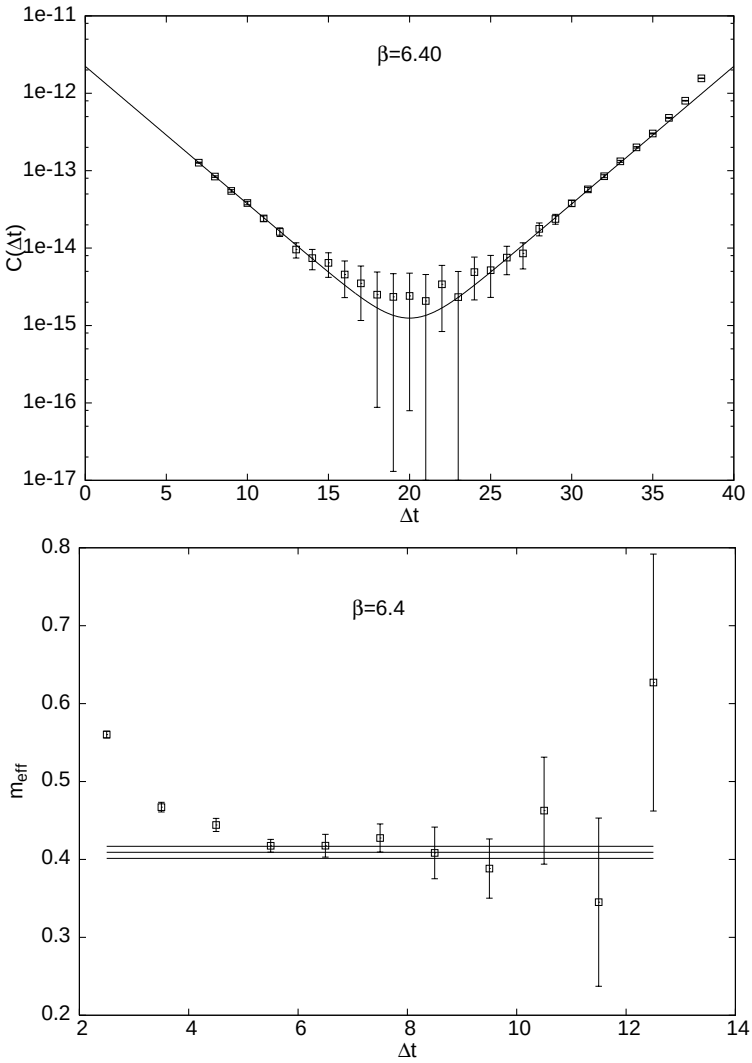

Figure 6.7: The correlator along with it's fit (fit range: 8-16) and the effective mass plot at the $\beta = 6.4$ for the scalar channel.

For $\beta = 6.4$ we compared our data with table 1 of [3]. At $\beta = 6.4$ [3] reports the value of scalar glueball mass $ma = 0.3960(93)$. From the global fit of the correlator we obtain the value of scalar glueball mass $ma = 0.4091(77)$. Excited state effects seem to be present till about $\Delta t = 5$

.

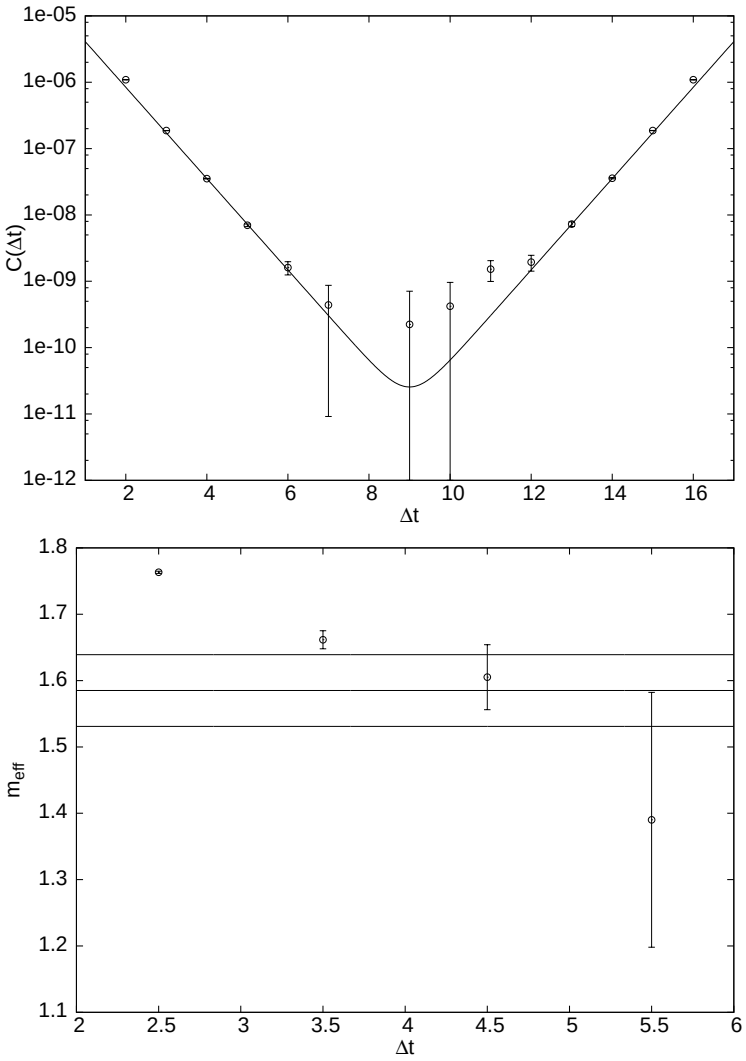

Figure 6.8: The correlator along with it's fit (fit range : 4-7) and the effective mass plot at the $\beta = 5.8$ for the tensor channel.

In the tensor channel at $\beta = 5.8$, we look at two lattices ($8^3 \times 18$ and $12^3 \times 18$) with different spatial volumes. Unfortunately the data was noisy and we did not get a signal for correlators beyond Δt of 7. At this β, we report the results from the operator $\mathcal{E}_2$ as the corresponding correlators were less noisy. For the $8^3 \times 18$ lattice we obtain $ma = 1.525(35)$ and for the $12^3 \times 18$ lattice we get $ma = 1.585(54)$. This is in the same ball park as the values reported in [1] viz. $ma = 1.52(5)$ at $\beta = 5.7995$ and $ma = 1.57(6)$ at $\beta = 5.8$ both at spatial volumes of 10^3.

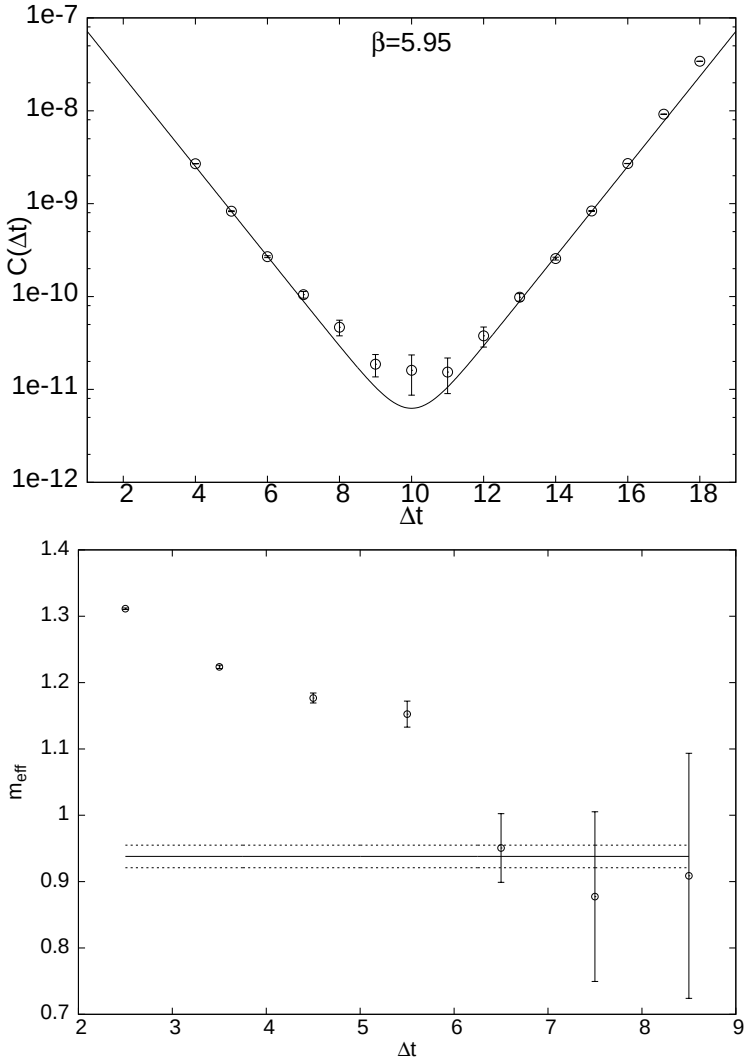

Figure 6.9: The correlator along with it's fit (fit range : 6-10) and the effective mass plot at the $\beta = 5.95$ for the tensor channel.

At $\beta = 5.95$, interpolating the data in [1] between $\beta = 5.8945$ and $\beta = 6.0625$ we get $ma = 1.148(19)$ for the tensor mass. Our best estimate gives $ma = 0.938(17)$ for the fit range between $\Delta t = 6$ and $\Delta t = 10$. However if we include the point $\Delta t = 5$ in our fit, the mass changes to $ma = 1.115(39)$. The same trend is there in the effective masses as well. Between $\Delta t = 5$ & 6, am_{eff} jumps from around 1.15 to 0.95.

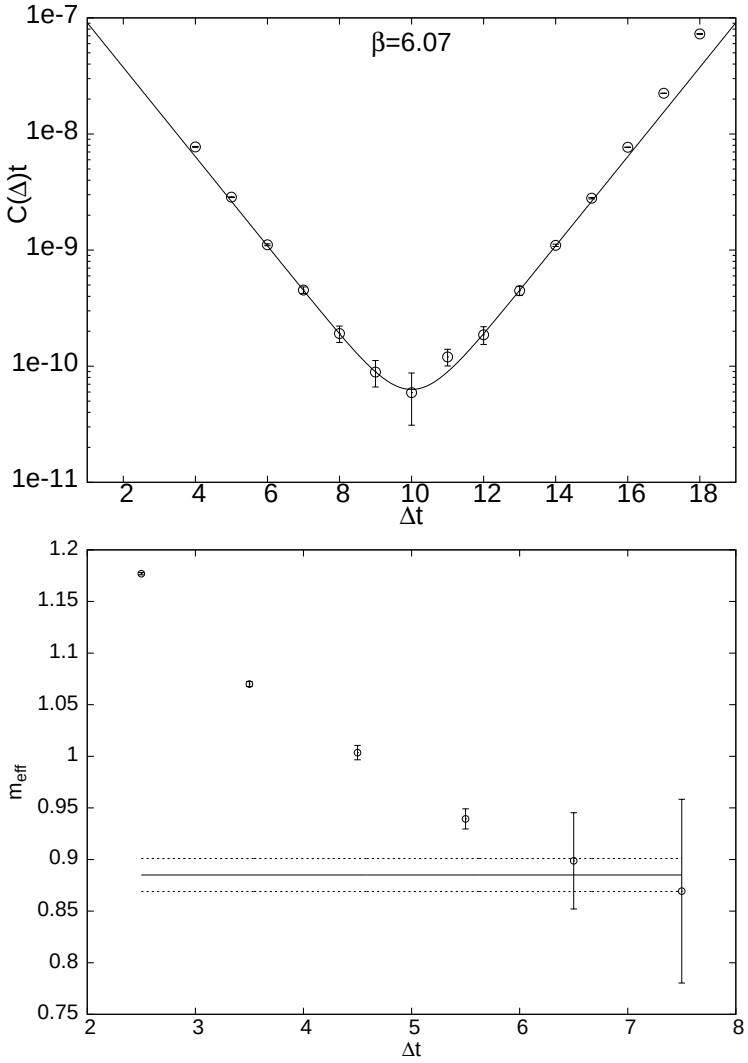

Figure 6.10: The correlator along with it's fit (fit range : 6-10) and the effective mass plot at the $\beta = 6.07$ ($L = 12$)for the tensor channel.

At $\beta = 6.07$, we have results from two different lattices *viz.* F and G. This therefore serves as a check on finite volume effects. From the smaller lattice with volume $12^3 \times 20$ we obtain $ma = 0.885(16)$ and the effective masses are consistent with that. The value reported in [1] is 0.922(13) at $\beta = 6.0625$ and interpolation gives $ma = 0.913(13)$ at $\beta = 6.07$, consistent within errorbars with our value. At $\beta = 6.07$ our results are from the operator $\mathcal{E}_1$. Contamination from excited states seems to persist till $\Delta t = 6$.

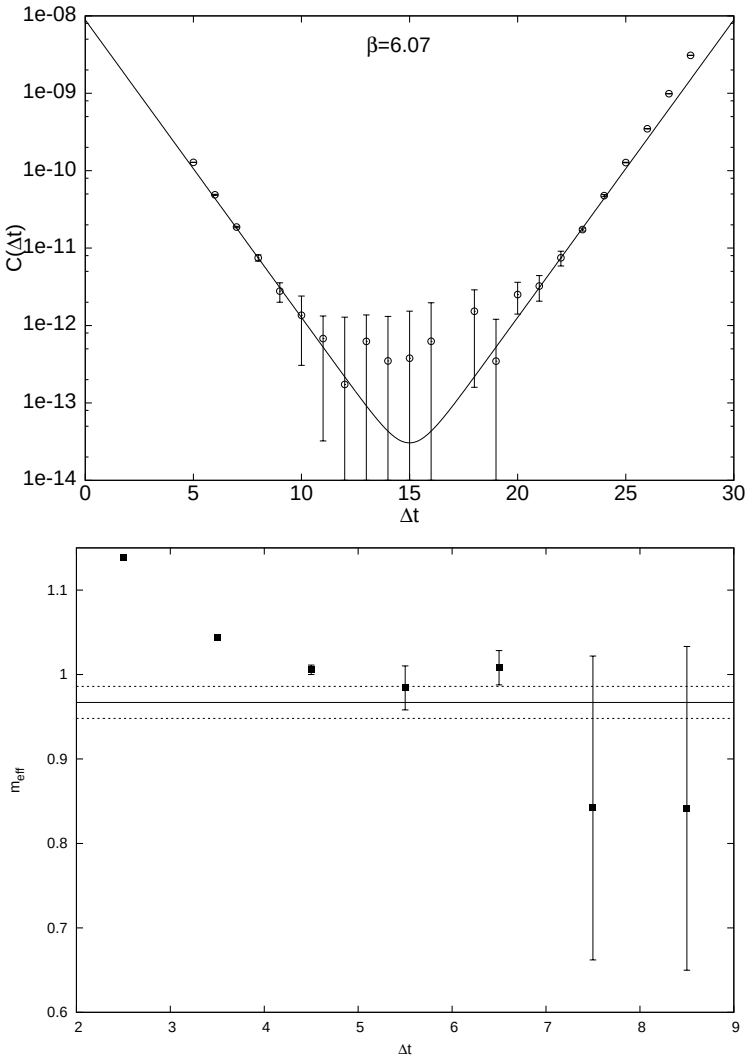

Figure 6.11: The correlator along with it's fit (fit range : 7-9) and the effective mass plot at the $\beta = 6.07$ ($L = 18$)for the tensor channel.

From our larger lattice with volume $18^3 \times 30$, we obtain $ma = 0.967(19)$, which is in complete agreement with calculation at $L = 12$ but with only half the error. On this lattice the effective mass plots indicate significant contamination from excited states till $\Delta t = 7$.

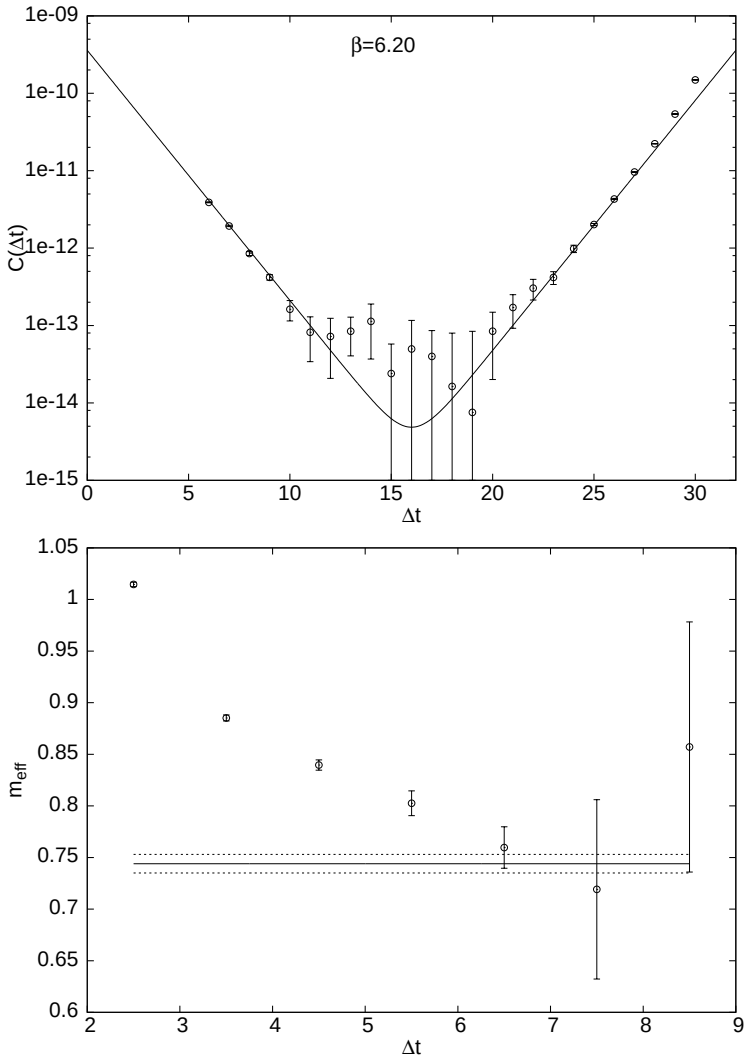

Figure 6.12: The correlator along with it's fit (fit range : 6-10) and the effective mass plot at the $\beta = 6.20$ for the tensor channel.

For $\beta = 6.2$ we compared our data with table 1 of [3]. At $\beta = 6.2$ [3] reports the value of tensor glueball mass $ma = 0.7784(74)$. From the global fit of the correlator (using operator $\mathcal{E}_2$) we obtain the value of scalar glueball mass $ma = 0.744(9)$. Contamination due to excited states seem to persist till $\Delta t = 6$.

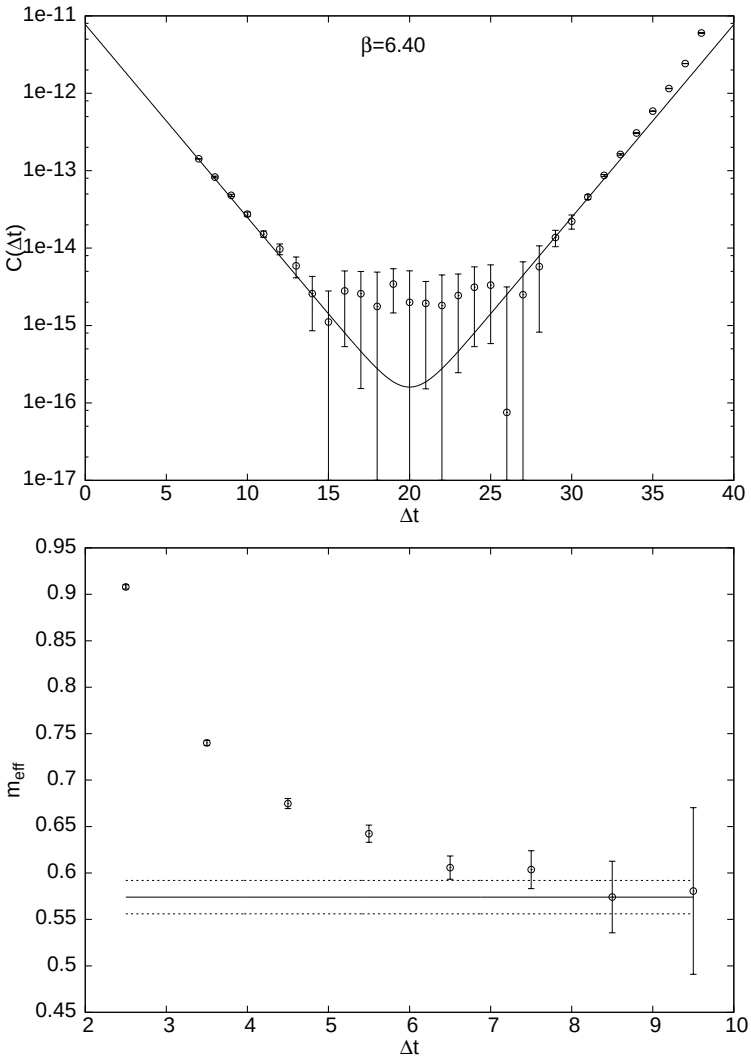

Figure 6.13: The correlator along with it's fit (fit range : 10-13) and the effective mass plot at the $\beta = 6.4$ for the tensor channel.

For the tensor channel at $\beta = 6.4$ we obtained (using operator $\mathcal{E}_2$) from global fit $ma = 0.574(18)$. While [3] reports the tensor glueball mass $ma = 0.5758(32)$ at the same value of β. Excited state contribution seem to persist till $\Delta t = 8$ in this case.

Correlated fit for the Tensor Channel					
	correlated fit			effective mass	
#	range	ma	$\frac{\chi^2}{d.o.f}$	t-slice	ma
	5-9	0.988(5)	0.1-0.74	2/3	1.139(1)
	6-9	0.985(10)	0.16-1.0	3/4	1.044(2)
G			0.38	4/5	1.006(6)
				5/6	0.984(26)
				6/7	1.008(20)
				7/8	0.842(180)
				8/9	0.842(192)
	6-10	0.721(9)	1.6-3.1	2/3	1.015(2)
	7-10	0.810(46)	0.35-1.6	3/4	0.885(3)
	8-10	0.780(70)	0.37-2.3	4/5	0.840(5)
H	8-11	0.796(53)	0.25-1.37	5/6	0.802(12)
				6/7	0.760(20)
				7/8	0.719(87)
				8/9	0.857(121)
			0.19	2/3	0.911(2)
	8-13	0.603(22)	0.15-0.55	3/4	0.742(3)
	9-13	0.598(51)	0.2-0.69	4/5	0.673(6)
	10-13	0.543(69)	0.001-0.36	5/6	0.649(9)
I	11-13	0.624(240)	0.006-0.35	6/7	0.638(16)
				7/8	0.625(26)
				8/9	0.643(59)
				9/10	0.722(153)

Table 6.6: Glueball masses for the tensor channel in lattice units (a denotes the lattice spacing) for all lattices along with the fit parameters.

β	ma	L	mL	mr_0
5.7*	0.952(11)	10	9.52(11)	2.78(4)
5.6993	0.969(18)	8	7.75(14)	2.83(6)
5.6925	0.941(25)	8	7.53(20)	2.70(8)
5.8*	0.906(8)	12	10.87(10)	3.328(34)
5.8	0.945(21)	10	9.45(10)	3.471(82)
5.7995	0.909(15)	10	9.09(15)	3.335(60)
5.95∗	0.7510(15)	16	12.016(24)	3.678(16)
5.95†	0.743(12)	-	-	3.639(68)
6.07∗	0.596(5)	18	10.73(9)	3.597(40)
6.07†	0.6301(77)	-	-	3.801(57)
6.2∗	0.503(8)	24	12.07(19)	3.712(72)
6.2	0.5197(51)	20	10.39(10)	3.835(38)
6.4∗	0.4091(77)	30	12.27(23)	3.985(95)
6.4	0.3960(93)	28	11.09(26)	3.857(91)

Table 6.7: Comparison of scalar glueball masses. A $*$ on the β indicates that it is from this work. Other entries are from [1]. A † on the β indicates that the corresponding mass was obtained by exponential interpolation between neighbouring β values reported in [1]. r_0 for β values in [1] were obtained by interpolating and extrapolating the values presented in [9]. For $\beta = 6.2$ and 6.4 we compared with table 1 of [3].

β	ma	L	mL	mr_0
5.8*	1.525(35)	8	12.20(28)	5.60(14)
5.8*	1.585(54)	12	19.02(65)	5.82(21)
5.8	1.57(6)	10	15.7(6)	5.77(23)
5.7995	1.52(5)	10	15.2(5)	5.58(19)
5.95*	1.115(39)	12	11.26(20)	5.46(21)
$5.95^{\dagger}$	1.148(19)	-	-	5.62(11)
6.07*	0.967(19)	18	17.41(34)	5.83(13)
$6.07^{\dagger}$	0.913(13)	-	-	5.51(9)
6.0625	0.922(13)	16	14.75(21)	5.56(9)
6.2*	0.744(9)	24	17.86(22)	5.49(9)
6.2	0.7784(74)	20	15.57(16)	5.745(58)
6.4*	0.574(18)	30	17.22(54)	5.59(20)
6.4	0.5758(32)	28	16.12(9)	5.608(80)

Table 6.8: Comparison of tensor glueball masses. Labelling convention is identical to 6.7. For $\beta = 6.2$ and 6.4 we compared with table 1 of [3].

Bibliography

[1] B. Lucini, M. Teper, U. Wenger, *JHEP* **0406** (2004) 012 [arXiv:hep-lat/0404008].

[2] S. Necco and R. Sommer, *Nucl. Phys.* **B622** (2002) 328.

[3] I. Montvay, G. Münster, *"Quantum Fields on a Lattice"*, Cambridge University Press, Cambridge 1994.

[4] H. B. Meyer, *JHEP* **0301** (2003) 048 [arXiv:hep-lat/0209145].

[5] H. B. Meyer, *JHEP* 0401 (2004) 030 [arXiv:hep-lat/0312034].

[6] H. B. Meyer, *JHEP* **0901** (2009) 071 [arXiv:hep-lat/0808.3151].

[7] M. Della Morte, L. Giusti, *JHEP* **1105** (2011) 056 [arXiv:hep-lat/1012.2562].

[8] M. Guagnelli, R. Sommer and H. Wittig, *Nucl. Phys.* **B535** (1998) 389 [arxiv:hep-lat/9806005].

Chapter 7

Finite Volume Effects

Error reduction techniques only reduce statistical errors. There are systematic errors as well and the most important among that are finite volume effects. In our lattices with small physical volumes (B_1 to F_1), we encounter them.

In lattice gauge theory simulations the number of lattice points N_x, N_y, N_z, N_t are restricted by available computer resources. In order to extrapolate to the continuum limit of lattice calculations, one needs to consider lattice spacings small relative to the correlation length so that scaling behaviour is at least approximately realized. The ratio of correlation length ξ to the lattice spacing a, and the ratio of the linear size of the lattice L to the correlation length ξ are two important geometrical characteristics of the lattice simulations. The finite size of the lattice has strong effects on the measurable quantities for $\xi \sim L$. These are called finite volume effects.

The nature of finite-volume effects depends very much on the theory under consideration. In the case of asymptotically free theories in a finite volume, like pure non-Abelian gauge theories in four dimensions, it is known [1] that for small volumes the relevant parameter is a running coupling $g(1/L)$ associated with the scale $1/L$. Owing to asymptotic freedom, this coupling becomes small for very small volumes, which makes it possible to calculate volume dependent quantities by means of perturbation theory in the small-volume limit [2, 3].

In [2] M. Lüscher proposed a method for the universal expansion for the masses of the low-lying stable particles in asymptotically free theories. The method is based on the observation that the energy spectrum of field theories in a box is discrete and peturbatively computable. In another work [3] Lüscher showed that the expansions for the lowest-lying energies of SU(N) theory are given by

$$E = \frac{1}{L}\sum_{k=0}^{\infty} \varepsilon_k \overline{\lambda}^k, \qquad \overline{\lambda} = [\overline{g}(\Lambda_{\overline{MS}})]^{2/3} \tag{7.1}$$

and these energies are exactly equal to a quantum mechanical effective Hamiltonian H'. The effective Hamiltonian H' acts on the wave function of constant gauge potentials

$$A_k^a, \qquad k = 1, 2, 3; \qquad a = 1, ..., N^2 - 1. \tag{7.2}$$

The expansion for the H' is that

$$H' = \frac{\overline{\lambda}}{L} \sum_{\nu=0}^{\infty} \overline{\lambda}^{\nu} H'_{\nu} \tag{7.3}$$

with

$$H'_0 = \frac{1}{2} \frac{\partial^2}{\partial A_k^a \partial A_k^a} + \frac{1}{4} (f^{abc} A_k^b A_l^c)(f^{ade} A_k^d A_l^e), \tag{7.4}$$

$$H'_1 = a_1 A_k^a A_k^a, \tag{7.5}$$

$$H'_2 = 0, \tag{7.6}$$

$$H'_3 = a_2 H'_0 + a_3 s^{abcd} A_k^a A_k^b A_l^c A_l^d + a_4 [5 A_k^a A_k^b A_k^c A_k^d - 3 A_k^a A_k^b A_l^c A_l^d]. \tag{7.7}$$

The numerical constants a_i are given by

$$a_1 = -\frac{N}{4\pi} \times 1.89153165, \tag{7.8}$$

$$a_2 = -\frac{11N}{9(4\pi)^2} \times 0.409052802, \tag{7.9}$$

$$a_3 = \frac{2}{15(4\pi)^2}, \tag{7.10}$$

$$a_4 = -\frac{1}{5(4\pi)^2} \times 0.619331710. \tag{7.11}$$

f^{abc} are the $SU(N)$ structure constants and s^{abcd} are totally symmetric invariant tensors defined by,

$$s^{abcd} = \frac{1}{12} N (d^{abc} d^{ecd} + d^{ace} d^{ebd} + d^{ade} d^{ebc}) + \frac{2}{3} (\delta^{ab} \delta^{cd} + \delta^{ac} \delta^{bd} + \delta^{ad} \delta^{bc}) \tag{7.12}$$

Following the method of Lüscher and Münster, P. Weisz and Zeiman [4] calculated the eigenvalues of this effective Hamiltonian by using the Rayleigh-Ritz variational principle. A basic harmonic function of the form

$$\psi(A) = Q(A) \exp(-\frac{1}{2} \omega A_k^a A_k^a), \tag{7.13}$$

was used as trial wave function, where $Q(A)$ is a polynomial in the A's having appropriate transformations for a given J^{PC} and ω is a variational parameter. In a second step the perturbations H'_{ν}, $\nu \geq 1$ are treated according to standard Rayleigh-Schrödinger

perturbation theory.
An interesting result found from the diagonalisation of the Hamiltonian was that, at very small volumes the lowest state is the 2^{++} followed by the state 0^{++}. This feature was first seen by the Monte Carlo study of finite size effects by C. Michael and M. Teper [2]. We also see this feature in our studies for smaller lattices. As it can be seen from table 7.1 and table 7.2 that at $\beta = 5.8$ the mass in the tensor channel is smaller than the mass in the scalar channel which is the expected behaviour at small volumes [3, 6, 7]. The lattice calculations show very different finite size behaviour for the A_1^{++} and E^{++} glueball masses. The results [2] for the A_1^{++} glueballs are rather independent of the size L of the lattice , while the E^{++} data show an abrupt change around $L = 9$.

Information about the finite size effects can be extracted from the plot of the dimensionles mass ratios (e.g. ratio of glueball mass in any channel to the glueball mass in the A_1^{++} channel) versus $z = mL$. Such a plot obtained by C. Michael and M. Teper [2] is depicted in Fig. 7.1.

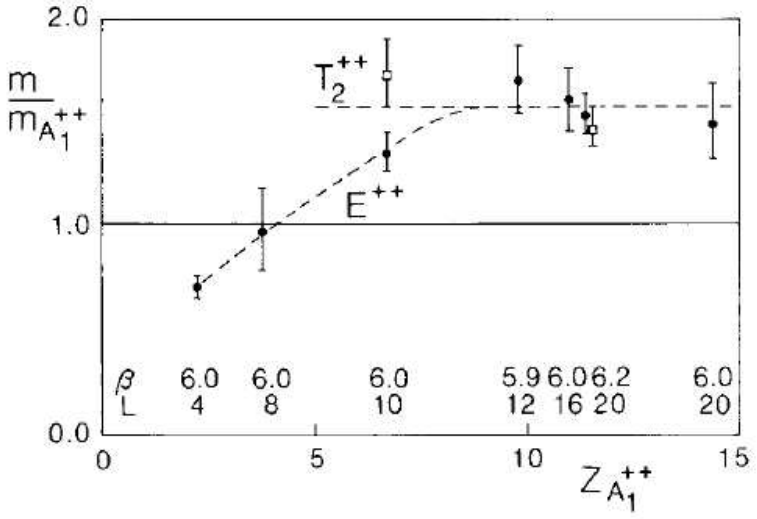

Figure 7.1: Ratios of glueball masses to the A_1^{++} mass plotted against the dimensionless spatial size variable $z = mL$. The E^{++} glueball was lightest for $z < 5$.

Findings from [2] was that for z > 9 there appear to be no finite-size effects for the glueball mass estimation. For a more recent study of finite volume effects in glueball masses see [8].

Lattice	β	z	ma	χ^2/dof
$6^3 \times 16$	5.7	5.54	0.924(33)	1.41
$6^3 \times 18$	5.8	3.63	0.605(12)	0.36
$8^3 \times 24$	5.95	3.11	0.389(17)	1.8

Table 7.1: Scalar glueball masses from very small volume calculations.

Lattice	β	z	ma	χ^2/dof
$6^3 \times 18$	5.8	3.63	0.476(31)	0.49
$8^3 \times 30$	5.95	3.11	0.444(25)	0.22

Table 7.2: Tensor glueball masses from very small volume calculations.

In our work we therefore kept $mL > 9$ in all cases.

Bibliography

[1] G. Münster, *Z. Phys.* **C12** (1982) 43.

[2] M. Lüscher, *Nucl. Phys.* **B205** (1982) 483.

[3] M. Lüscher, *Nucl. Phys.* **B219** (1983) 233.

[4] P. Weisz, V. Zieman, *Nucl. Phys.***B284** (1987) 157-170.

[5] C. Michael, M. Teper, *Nucl. Phys.* **B314** (1989) 347-362.

[6] M. Lüscher, G. Münster, *Nucl. Phys.* **B232** (1984) 445.

[7] P. Weisz, V. Ziemann, *Nucl. Phys.* **B284** (1987) 157.

[8] H. B. Meyer, *JHEP* 0503 (2005) 064 [arXiv:hep-lat/0412021].

Chapter 8

Continuum Limit Extrapolation

As the space-time lattice introduces an UV cut off to the theory, it is important to get a continuum extrapolation of lattice observables. As the regulator is removed, observable quantities should approach their physical values.

8.1 Continuum Limit of Lattice Gauge Theory

In chapter 2 we have seen that Wilson's gauge action has a naive Continuum limit. There are various possibilities of formulating gauge actions with the same continuum limit. One can also use different definitions of derivatives for the lattice actions. However the physical observables in different formulations should agree with experimentally measured values in $a \to 0$ limit. This implies that the bare coupling should depend non-trivially on a. On the lattice, dimensionless quantities such as masses in lattice unit $\hat{m} = am$ are convenient to calculate. The physical mass m of the continuum field theory should remain finite, which implies that the mass $\hat{m}$ measured in lattice units of the corresponding lattice field theory must vanish in continuum limit. The correlation length in lattice units is defined as,

$$\xi = \frac{1}{am}. \tag{8.1}$$

Therefore correlation lengths in lattice units must diverge in the continuum limit. In pure gauge theory the bare coupling g_0 is the only free parameter of the action. The study of the lattice system near the continuum limit requires a tuning parameter, in this case $g_0 = g_0(a)$.

Let $\Theta(g_0(a), a)$ be a physical observable in pure lattice gauge theory. The bare parameter $g_0(a)$ should depend on a in such a way that Θ should agree with the

experimental value of the observable Θ_0 in the limit

$$\lim_{a\to 0} \Theta(g_0(a), a) = \Theta_0. \tag{8.2}$$

The continuum theory is independent of the regularization parameter; this leads to renormalization group equation

$$\frac{d}{d(\ln a)}\Theta(g_0(a), a) = 0 \tag{8.3}$$

or, equivalently

$$\frac{\partial}{\partial(\ln a)}\Theta(g_0(a), a) + \frac{\partial g}{\partial(\ln a)}\frac{\partial}{\partial g}\Theta(g_0(a), a) = 0 \tag{8.4}$$

The renormalization group function (β-function) is defined as

$$\beta(g_0) = -\frac{\partial g_0}{\partial(\ln a)}. \tag{8.5}$$

Knowledge of the β-function determines the cut-off dependence of the bare parameter $g_0(a)$. For small g_0 the expansion of the β-function around g_0 is the following

$$\beta(g_0) = -\beta_0 g_0^3 - \beta_1 g_0^5 + \mathcal{O}(g_0^7). \tag{8.6}$$

Where the coefficients β_0, β_1, ... are determined by perturbative calculations. In general the precise form of β-function is dependent on the renormalization scheme. For $SU(N_c)$ pure gauge theory the first two coefficients are given by

$$\beta_0 = \frac{11}{3(4\pi)^2}N_c \tag{8.7}$$

$$\beta_1 = \frac{34}{3(4\pi)^4}N_c^2 \tag{8.8}$$

Solving eq. 8.5 and eq. 8.6 in this approximation one obtains

$$a(g_0) = \frac{1}{\Lambda_L}(\beta_0 g_0^2)^{-\frac{\beta_1}{2\beta_0^2}} \exp(-\frac{1}{2\beta_0 g_0^2})(1 + \mathcal{O}(g_0^2)) \tag{8.9}$$

where Λ_L is an integration constant, which depends on the renormalization scheme. Inverting the previous relation one obtains

$$g_0(a)^{-2} = \beta_0 \ln(a^{-2}\Lambda_L^{-2}) + \frac{\beta_1}{\beta_0}\ln(\ln(a^{-2}\Lambda_L^{-2})) + \mathcal{O}(1/\ln(a^2\Lambda_L^2)). \tag{8.10}$$

Eq. 8.9 and eq. 8.10 show that the limit $a \to 0$ corresponds to vanishing coupling g_0, which shows that the critical point is reached at $g_0 = 0$. The point $g_0 = 0$ is also the fixed point of the renormalization group equation. This is consistent with the fact

that the zeros of the β-function, representing ultraviolet-attractive fixed points, must be universal if the continuum limit is unique.

The dependence of bare coupling on the lattice constant suggests that, to obtain continuum limit $a \to 0$, we have to study the limit

$$\beta \to \infty \tag{8.11}$$

where β is the lattice coupling. One needs additionally to take the so-called thermodynamic limit

$$N \to \infty, \quad N_T \to \infty, \tag{8.12}$$

to obtain the limit (8.11). Since taking this limit is not practical, one often calculates physical observables for a few values of β, corresponding to different values of a. The numbers of lattice points N, N_T can be chosen in such a way that, physical volumes remain fixed for different values of a. One can analyse the scale dependence of the observables and extrapolate to the limit $a \to 0$, by studying the results for different a at a fixed physical volume. The study of a-dependence of the observables is known as scaling analysis.

8.2 Setting the Scale

In order to perform the continuum extrapolation presented in section 8.1 and to assess the size of lattice artifacts present in different discretizations one needs a gluonic reference scale. In the lattice formalism all observables are dimensionless. Only by relating them to physical quantities may we introduce such a reference scale. The product of the lattice spacing a and some mass M is an example of such dimensionless quantities on the lattice. Identifying the mass M with a physical mass, one can determine the lattice constant a in physical units.

An alternative method for scale setting [9] uses a reference scale tied to the static quark potential. This reference scale often denoted by r_0 is known as the Sommer parameter. This is the preferred method to set the scale in pure Yang-Mills theory and we follow this scale setting.

8.2.1 Determination of r_0

Determination of the Sommer scale r_0 is not based directly on the potential $V(r)$, but instead on the force $F(r) = -\frac{dV(r)}{dr}$ between two static quarks. Let us consider the

planar Wilson loop of size $r \times t$. The spatial distance r and the Euclidean time t are related to integer numbers n and n_t through the lattice spacing a,

$$r = na, \quad t = n_t a \tag{8.13}$$

The static potential $V(r)$ can be determined from the vacuum expectation values of the Wilson loop in the confined phase using,

$$\langle W_c \rangle = C \ \exp(-tV(r)) = C \ \exp(-n_t a V(na)). \tag{8.14}$$

The dimensionless quantity $aV(an)$ at different n can be determined from the numerical data for $\langle W_c \rangle$. In practice this is done via a two-parameter fit to the data for different n_t (but fixed n) according to (8.14). The fit parameters are C and $aV(an)$. Repeating this procedure for different values of n, one can get a set of numerical data for $aV(an)$ as a function of n.

In terms of the static potential the Sommer parameter is defined by,

$$r_0^2 F(r_0) = 1.65, \tag{8.15}$$

which corresponds to $r_0 \simeq 0.5$ fm. One can determine the value $r = r_0$ by calculating the dimensionless product $r^2 F(r)$ where this product assumes the value 1.65.

In [9] the lattice spacing a was determined for several values of β and the dependence of a on β was parametrized for $5.7 \leq \beta \leq 6.57$ as

$$\ln(a/r_0) = -1.6805 - 1.7139(\beta - 6) + 0.8155(\beta - 6)^2 - 0.6667(\beta - 6)^3. \tag{8.16}$$

The form of the parametrization in eq. 8.16 is inspired by the renormalization group equation. We used the values in [9] to set the scale in this work.

8.3 Towards the Continuum Limit of Glueball Masses

In this section we will discuss continuum extrapolations of the glueball masses. Lattice spacings in numerical simulations may be so small that the lattice artifacts are numerically negligible. However the computational resources available at present for numerical simulations are not sufficient to produce negligible lattice artifacts. The knowledge of lattice artifacts have practical and theoretical importance. In lattice calculations we usually make extrapolations of the ratios of the masses of the form

$$\frac{m_1(a)}{m_2(a)} \to \frac{m_1(0)}{m_2(0)} + \mathcal{O}(a^p) \tag{8.17}$$

assuming leading artifacts are predominantly polynomial in the lattice spacing. The lattice artifacts are non-universal i.e., the exponent p depends on the lattice action. Most of our analytical knowledge of lattice artifacts stems from investigations in the framework of perturbation theory. Using the knowledge of lattice artifacts for a particular lattice action one can get continuum limit extrapolations of lattice observables.

The continuum extrapolations of the scalar and tensor glueball masses prior to our work is depicted in Figs. 8.1 and 8.2.

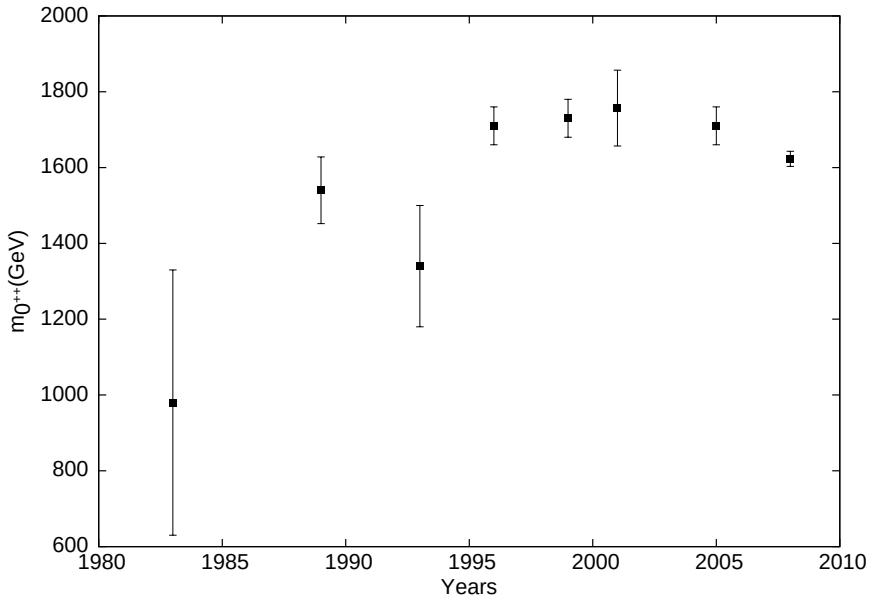

Figure 8.1: Continuum scalar glueball masses over the years [1–3, 3–7].

β	r_0/a	fit range	ma	mr_0
5.7	2.922(9)	$1.71r_0$-$3.08r_0$	0.952(11)	2.78(4)
5.8	3.673(5)	$1.63r_0$-$2.45r_0$	0.906(8)	3.328(34)
5.95	4.898(12)	$1.02r_0$-$2.04r_0$	0.7510(15)	3.678(16)
6.07	6.033(17)	$0.83r_0$-$1.65r_0$	0.617(7)	3.722(52)
6.2	7.380(26)	$0.81r_0$-$1.63r_0$	0.537(11)	3.963(95)
6.4	9.74(5)	$0.82r_0$-$1.64r_0$	0.4091(77)	3.985(95)

Table 8.1: Scalar glueball masses considered for the continuum extrapolation.

We computed the glueball masses for the scalar channel for $\beta = 5.7, 5.8, 5.95, 6.07, 6.2$ and 6.4. For the tensor channel the glueball correlator was too noisy for a reliable extraction of the glueball mass for $\beta = 5.7$. So we extracted tensor glueball masses

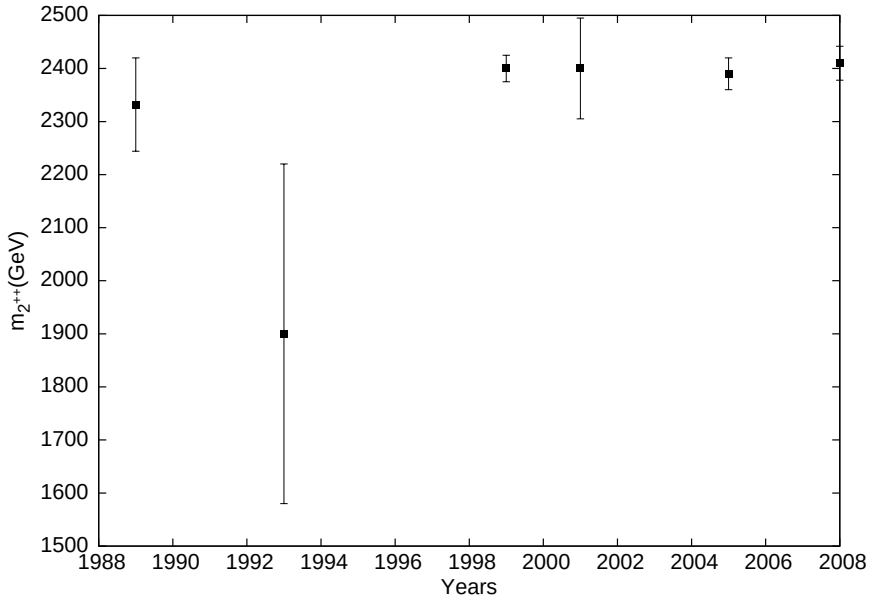

Figure 8.2: Continuum tensor glueball masses over the years [2, 3, 3, 5–7].

β	r_0/a	fit range	ma	mr_0
5.8	3.673(5)	$1.09r_0$-$1.91r_0$	1.585(54)	5.82(21)
5.95	4.898(12)	$1.22r_0$-$2.04r_0$	1.115(39)	5.46(21)
6.07	6.033(17)	$0.99r_0$-$1.65r_0$	0.967(19)	5.83(13)
6.2	7.380(26)	$0.81r_0$-$1.36r_0$	0.744(9)	5.49(9)
6.4	9.74(5)	$0.82r_0$-$1.64r_0$	0.574(18)	5.59(20)

Table 8.2: Tensor glueball masses considered for the continuum extrapolation.

for $\beta = 5.8, 5.95, 6.07, 6.2$ and 6.4. We have seen in ch. 6 that the extracted glueball masses varies with the fit range. The effective mass plots in ch. 6 give an estimate for the fit range to extract glueball masses. We have tried as much as possible to extract glueball mass from same fit range in physical units for all the lattice spacings. For the scalar channel we extracted the masses from fit range $0.85r_0 - 1.65r_0$. For the tensor glueballs we were not able to fix a uniform range. While for β =6.07 and 6.4 we could extend the fit range to about $1.6r_0$, for β =6.2 our largest distance was $1.3r_0$. The best estimates for the glueball masses and corresponding fit ranges in physical units are given in table. 8.1 and 8.2. Our plots for the best estimates of scalar and tensor glueball masses are illustrated in figure 8.3. We compared these calculations with two recent works by Harvey Meyer [8] and Harindranath *et al.* [10]. To get an idea about the continuum limit for the glueball masses we plotted(fig. 8.4 and 8.5) our results

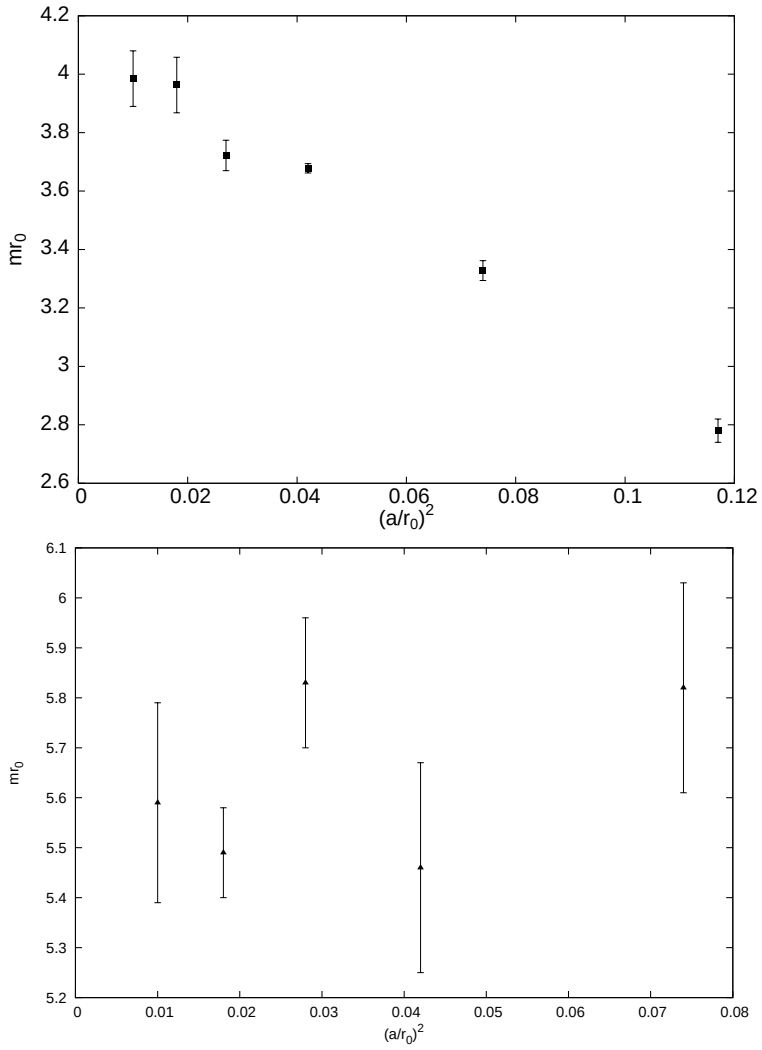

Figure 8.3: Scalar and tensor glueball masses plotted against $(a/r_0)^2$. The figure at the top is for scalar channel while the bottom figure is for tensor channel.

together with results from [8] and [10].

The combined plot for the scalar masses seem to indicate a rise in the masses upto $\beta = 6.07$ while the finer lattices seem to indicate a flat behaviour with mr_0 extrapolating to a value between 3.8 and 4. The errorbars on the results for tensor masses from our results and [8] show a more scattered behaviour over the range of β explored. The complicated lattice spacing dependence of the measured glueball masses makes extrapolation to the continuum limit difficult. If however one combines the masses from our results and [8], the variation of masses with β seems quite flat with mr_0 varying between 5.5 and 5.7.

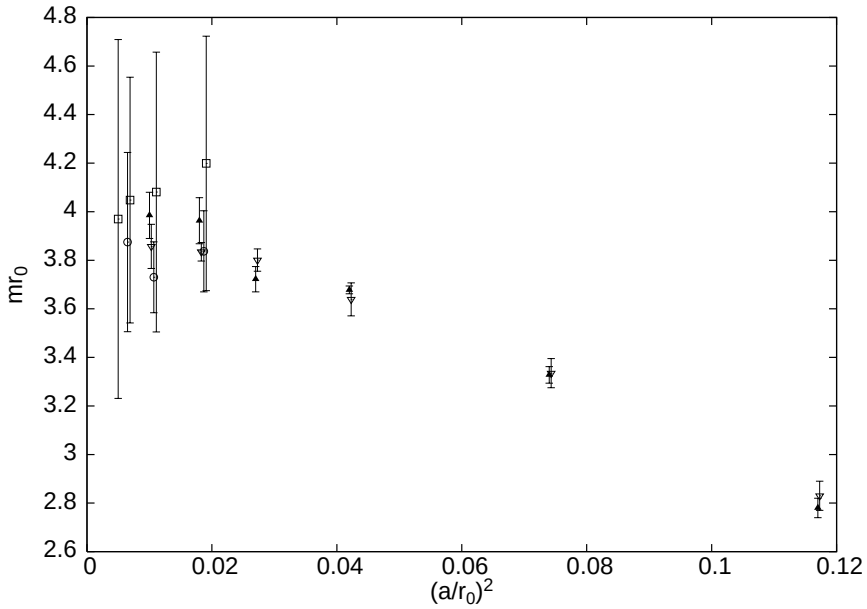

Figure 8.4: Scalar glueball masses plotted against $(a/r_0)^2$ together with results from [8] and [10]. Filled triangles are from our calculation and open triangles are from [8], squares are from calculations with open boundary conditions [10], circles are from calculations with periodic boundary conditions [10]

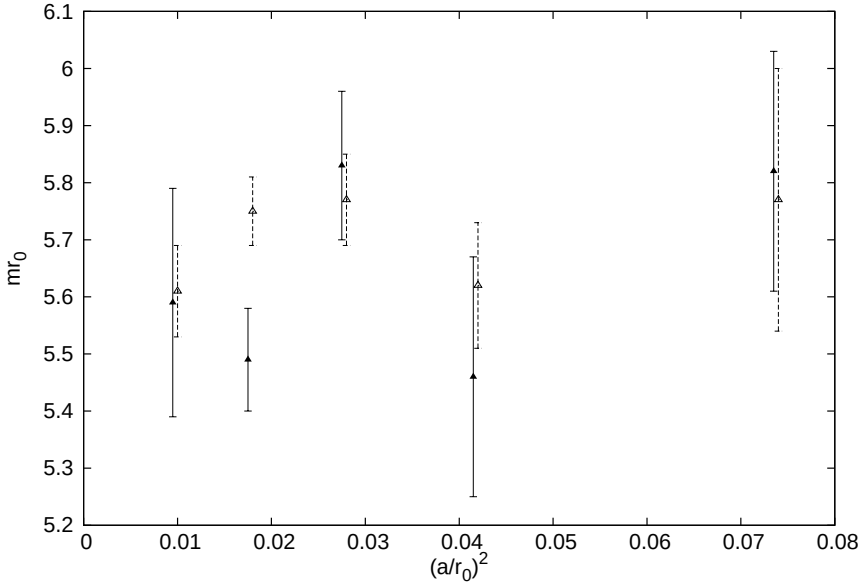

Figure 8.5: Tensor glueball masses plotted against $(a/r_0)^2$ together with results from [8]. Filled triangles are from our calculation and open triangles are from [8].

Bibliography

[1] B. Berg, A. Billoire, *Nucl. Phys.* B226 (1983) 405-416.

[2] C. Michael, M. Teper, *Nucl. Phys.* **B314** (1989) 347-362.

[3] H. Chen, J. Sexton, A. Vaccarino, D. Weingarten, [arXiv:hep-lat/9308010].

[4] Xiang-Qian Luo, Qi-Zhou Chen, *Mod. Phys. Lett.* **A11** (1996) 2435-2442 [arXiv:hep-ph/9604395].

[5] C. J. Morningstar and M. J. Peardon, *Phys. Rev.* **D60** (1999) 034509 [arXiv:hep-lat/9901004].

[6] L. Chuan, *Chin. Phys. Lett.* **18** (2001) 187.

[7] Y. Chen *et. al.*, *Phys. Rev.* **D73** (2006) 014516 [arXiv:hep-lat/0510074].

[8] H. B. Meyer, *JHEP* **0901** (2009) 071 [arXiv:0808.3151].

[9] M. Guagnelli, R. Sommer and H. Wittig, *Nucl. Phys.* **B535** (1998) 389 [arxiv:hep-lat/9806005].

[10] A. Chowdhury, A. Harindranath, J. Maiti, *JHEP* 1406 (2014) 067.

Chapter 9

Conclusion

Extraction of glueball masses from correlators is a difficult problem in lattice QCD due to a very low signal to noise ratio at large Euclidean times. In this thesis we present a new method, based on the multilevel scheme, to enhance the signal to noise ratio in glueball correators.

The multilevel algorithm is very efficient for calculating quantities with very small expectation values. Operators in the tensor channel have zero expectation values and are therefore ideal for direct evaluation. For scalar operators we have subtracted the non-zero vacuum expectation values from the operators to get the connected correlators directly.

Correlation functions between large loops have the advantage that they have much less contamination from excited states compared to those between elementary plaquettes and the large loops are less sensitive to UV fluctuations compared to the elementary plaquettes. Multilevel schemes allow us to estimate the expectation values of the large loops with very high precision.

The efficiency of the algorithm depends crucially on choosing the optimal parameters for the algorithm such as the sub-lattice thickness and updates. These depend on β quite strongly. In the range of β we explored it seems that 0.5 fermi seems to be close to optimal for both the loop size and the thickness of the sub-lattice.

We observe that this error reduction technique works quite well at least in pure gauge theories. For a given computational cost, the improvement over the naive method in the signal to noise ratio is several times to more than an order of magnitude. We are able to follow the correlator to temporal separations of about 1 fermi and can perform global fits to the correlators between 0.5 and 1 fermi. Our effective masses also show a plateau in the same range obtained from the global fits.

It is of course of interest to reach the continuum limit. To get an idea about the estimate of continuum limit of glueball masses we performed our calculations for finer

lattices (up to $a = 0.051$ fm). For the scalar channel our results are in good agreement with two recent glueball mass calculations [3] and [4].

Although lattice discretization of Quantum Chromodynamics predicts glueballs, no glueballs have yet been discovered experimentally [1]. The particle data group (PDG) has listed following resonance states as glueball candidates

$$f_0(500),\ f_0(980),\ f_0(1370),\ f_0(1500),\ f_0(1710) \text{ and } f_J(2220)$$

where the last resonance states are candidate for the tensor channel glueball and the rests are candidates for the scalar channel glueball. The known spectra and multiplet assignment of the scalar and tensor states are listed in 9.1

Name	Mass[MeV/c^2]	Width[MeV/c^2]	Decays
$f_0(600)$	400-1200	600-1000	$\pi\pi, \gamma\gamma$
$f_0(980)$	980 ± 10	40-100	$\pi\pi, K\overline{K}, \gamma\gamma$
$f_0(1370)$	1200-1500	200-500	$\pi\pi, \rho\rho, \sigma\sigma, a_1\pi, \eta\eta, K\overline{K}$
$f_0(1500)$	1507±5	109±7	$\pi\pi, \sigma\sigma, \rho\rho, a_1\pi, \eta\eta, \eta\eta', K\overline{K}, \gamma\gamma$
$f_0(1710)$	1718±6	137±8	$\pi\pi, K\overline{K}, \eta\eta, \omega\omega, \gamma\gamma$
$f_2(1950)$	1944±12	472±18	$K^*\overline{K^*}, \pi\pi, 4\pi, a_2\pi, f_2\pi\pi, \eta\eta, K\overline{K}, \gamma\gamma$
$f_J(2220)$	2225-2235	15-30	$\gamma\pi\pi, \eta\eta'$

Table 9.1: Scalar and Tensor mesons as listed by the Particle Data Group [2].

A dedicated glueball search experiment is scheduled to begin shortly in GSI Darmstadt and we hope that the results from our calculation may help narrow the energy range for experimental search of scalar and tensor glueballs.

[1] For a recent review see [1]

Bibliography

[1] W. Ochs, *J. Phys.* **G40** (2013) 043001 [arXiv:hep-ph/1301.5183].

[2] J. Beringer *et al.* (Particle Data Group), *Phys. Rev.* **D86** (2012) 010001 [http://pdg.lbl.gov].

[3] H. B. Meyer, *JHEP* **0901** (2009) 071 [arXiv:hep-lat/0808.3151].

[4] A. Chowdhury, A. Harindranath, J. Maiti, *JHEP* 1406 (2014) 067 [arXiv:hep-lat/1402.7138].

List of Corrections

Sourav Mondal

1 Corrections

First, Considering the first comment of the examiner, I have added a statement mentioning the difficulty in an attempt to continuum extrapolation due to complicated lattice spacing dependence of measured glueball masses. Also the title of that section is modified as no continuum limit extrapolation attempted.

Second, Regarding the second comment of the examiner, we would like to point out that in section 6.1 it was mentioned that "Since it is not clear a-priori how the algorithm behaves as either Δt or β changes we report our experience for different values of Δt and β (see Table 6.2)". Generally it is known that the multilevel algorithm works better at stronger couplings (smaller values of β) than close to the continuum limit. We expect the same pattern to hold here as well.

Third, Taking into account the examiners comment, we have revised the value for the tensor channel glueball mass at $\beta = 6.07$ and $L = 18$. Originally for lattice G (Table 6.5) the result was quoted for the fit range $7 - 9$. In the corrected version the result is quoted for the fit range $6 - 9$, which has better $\chi^2/d.o.f.$ The corresponding mass plateau is changed in the effective mass plot **(Fig. 6.11)**. In the present form the error of the quoted result is compatible with the error of the effective mass. Corresponding changes in **Tables 6.8, 8.2** and in **Figs. 8.3, 8.5** are incorporated.

Two additional corrections are done in (i)**Table 6.8** and (ii) **Table 8.2**.

(i) In **Table 6.8** the value of mr_0 should be 5.56(9) instead of 5.49(9).

(ii)In **Table 8.2** the value of r_0/a for $\beta = 5.8$ should be 3.673(5) instead of 2.922(9).

Fourth, Clarification for the exponential interpolation eq.(6.6) is added in a footnote. A reference is also added for that clarification.

We have added a sentence to show how eq.(8.3) follows from eq.(8.2). In addition to that another minor correction have been made. In eq. 8.9 a minus sign was missing from the power of $(\beta_0 g_0^2)$, that correction have been incorporated.

Fifth, The corrections in the citations as suggested by the examiner have been incorporated as follows

1.) The reference of M. Lüscher and U. Wolff is added in chapter 5.

2.) In **Chapter 4** the citation for jackknife should be [5] instead of [17], that error is corrected.

3.) In **Fig. 8.4** comparison was with [8] and [10] instead of [3] and [4], that correction is done.

4.) In **Fig 8.5** the comparison was only with [8] instead of [3] and [4], that error is corrected.

5.) In the bibliography of **Chapter 8**, ref. 3 the author D. Weingarten is added and in ref. 8 "hep-lat" is removed as suggested by the examiner.

Other minor corrections :

1.)Definition of C_1 and C_2 is changed and a citation added for that definition.

2.)Eq.(2.13) is corrected according to the examiner's suggestion i.e., the summation over m and μ is added.

3.)The statement below eq.(4.5) as pointed out by the examiner is modified. It is stated that those two criterion are for any probability distributions.

In addition to that another typographical error is corrected in Chapter 4. Below the eq.(4.3) the reference for the probability distribution should be eq.(4.3) instead of eq.(5.4).

4.)Definition of N is given and the relation between inverse coupling β and the coupling g^2(used in Eq. (2.21) is given. That notation is used for the convenience of that chapter. Also the definition of staple A is corrected. In the second term of Eq.(4.14) $U_\nu^\dagger(n+\hat{\nu}-\hat{\mu})$ is replaced by $U_\nu^\dagger(n+\hat{\mu}-\hat{\nu})$
.

5.) We agree with the examiner's observation that a $SU(2)$ matrix always has determinant 1 and we have dropped the word "normalized" when referring to an $SU(2)$ matrix.

6.) In eq.(4.20) and (4.21) the $SU(2)$ matrix should be X instead of U, that corrections are incorporated.

7.) In eq.(7.1) the summation index should be k instead of ν, that error is corrected.

8.)In the caption of **Fig. 7.1** $L < 8$ is replaced by $z < 5$ as suggested by the referee.